Accepted Manuscript

Evolution of the Mozambique Belt in Malawi constrained by granitoid U-Pb, Sm-Nd and Lu-Hf isotopic data

Blackwell W.C. Manda, Peter A. Cawood, Christopher J. Spencer, Tony Prave, Ruth Robinson, Nick M.W. Roberts

PII: S1342-937X(18)30301-0
DOI: https://doi.org/10.1016/j.gr.2018.11.004
Reference: GR 2059

To appear in: *Gondwana Research*

Received date: 20 March 2018
Revised date: 21 September 2018
Accepted date: 7 November 2018

Please cite this article as: Blackwell W.C. Manda, Peter A. Cawood, Christopher J. Spencer, Tony Prave, Ruth Robinson, Nick M.W. Roberts , Evolution of the Mozambique Belt in Malawi constrained by granitoid U-Pb, Sm-Nd and Lu-Hf isotopic data. Gr (2018), https://doi.org/10.1016/j.gr.2018.11.004

Evolution of the Mozambique Belt in Malawi constrained by granitoid U-Pb, Sm-Nd and Lu-Hf isotopic data

*Blackwell W. C. Manda[1, 2], Peter A. Cawood [1, 3], Christopher J. Spencer[4], Tony Prave[1], Ruth Robinson[1], Nick M. W. Roberts[5].

[1] School of Earth and Environmental Sciences, University of St Andrews, St Andrews KY16 9AL, United Kingdom

[2] Department of Earth Sciences, Chancellor College, University of Malawi, Zomba, Malawi

[3] School of Earth, Atmosphere & Environment, Monash University, Melbourne, VIC 3800, Australia

[4] Earth Dynamics Research Group, The Institute of Geoscience Research (TIGeR), School of Earth and Planetary Sciences, Curtin University, Perth WA 6845, Australia

[5] NERC Isotope Geosciences Laboratory (NIGL), British Geological Survey, Keyworth, NG12 5GG, UK

*Corresponding Author,

Blackwell W. C. Manda,

University of Malawi,

Chancellor College,

Geography & Earth Sciences Department,

P. O. Box 280,

Zomba, Malawi.

Email: bmanda@cc.ac.mw

Tel: +265 881519384 (Mobile)

ABSTRACT

U-Pb, Sm-Nd and Lu-Hf isotopic data for granitoid rocks from southern Malawi provide constraints on the timing and sources of magmatic activity within this segment of the Mozambique Belt and its role in the Rodinia and Gondwana supercontinent cycles. LA-ICP-MS single zircon U-Pb ages indicate a number of periods of magmatic activity: late Mesoproterozoic at ca. 1130 Ma, 1070 Ma, and 1050 to 1030 Ma; Neoproterozoic at ca. 960 Ma and 600 Ma); Cambrian at ca. 530 and 515 Ma, and Mesozoic at ca. 120 Ma. The oldest igneous activity, 1128 ± 30 Ma, corresponds with emplacement of a charnockitic granitoid in the southeast corner of Malawi (Mulanje area). This region subsequently experienced metamorphism dated at 515 ± 18 Ma. The youngest magmatism is alkaline in affinity and is associated with the East African Rift.

Radiogenic isotope data indicate that the Mesoproterozoic samples have positive εNd and εHf values, signifying derivation from material with a suprachondritic signature, whereas the younger rocks have negative values suggestive of crustal material recycling and mixing for their source and origins. The data imply that in the Malawi region of the Mozambique Belt, addition of new crust occurred during Rodinia assembly whereas magmatic activity during Gondwana assembly was restricted to reworking and mixing.

KEYWORDS: MOZAMBIQUE BELT; GONDWANA; MALAWI; METAMORPHISM; DEPLETED MANTLE.

1. Introduction

Southern Malawi lies within the Mozambique Belt of the East African Orogen (Fig. 1). The orogen records the Neoproterozoic closure of an oceanic tract, the Mozambique Ocean, and subsequent collisional assembly of the continental fragments of East Gondwana (India, Madagascar, Antarctica, Australia) and West Gondwana (Africa, South America) (Meert et al., 1997; Meert 2003). The belt is also known as the East African–Antarctic orogen (Jacobs et al., 1998).

The East African Orogen stretches from the Arabian Nubian Shield in the north, along the East African margin (including the Mozambique Belt), into East Antarctica, a distance of over 8000 km, and is much as 1000 km in width (Muhongo et al., 1994; Stern, 1994; Jacobs et al., 2004). Within the region of Malawi and Mozambique, Holmes (1951) first applied the term Mozambique Belt, based on structural discontinuity between the Tanzanian craton and gneiss to the east. The northern part of the East African Orogen (i.e. in Egypt, Sudan, Eritrea, Ethiopia and northern Kenya) consists mainly of Neoproterozoic juvenile crust whereas its southern portion (i.e. central-south Kenya and Tanzania) is dominated by Neoproterozoic-age magmatism that is primarily comprised of reworked Neoarchean and Paleoproterozoic crust (Stern, 2002; Bingen et al., 2009; Thomas et al., 2016a). The latter regions are also considered to have experienced tectonothermal events associated with the end-Mesoproterozoic Kibaran orogeny (e.g. Andreoli, 1984; Sacchi et al., 1984; Daly, 1986).

In Malawi, there has been no systematic study of rocks that comprise the Mozambique Belt or characterisation of their isotopic fingerprints. The belt is orientated northwest–southeast and contains granitoid sheets intruded into a gneissic basement. The granitoids are mostly I-type and predominantly metaluminous with compositions spanning from granite and granodiorite to monzogranite and syenite (Andreolli, 1984; Kröner et al., 2001). In this paper, we present detailed zircon U-Pb and Lu-Hf and whole rock Sm-Nd and Lu-Hf isotope analyses of the main lithological units in the southern part of Malawi to refine understanding of the timing and nature of the tectonothermal events in the Mozambique Belt in this region, and its role in the Rodinia and Gondwana supercontinent cycles.

2. Geological background

Malawi lies at a key juncture in the zone of intersection and overlap between two fundamental sutures associated with Gondwana assembly, the East African (Mozambique Belt) and Kuunga orogens (Fig. 1; Meert et al., 1997; Meert 2003; Bingen et al., 2009). Older orogenic belts ascribed to Rodinia assembly, the Ubendian, Irumide (Kibaran), and Southern Irumide belts, are overprinted by the Mozambique Belt in adjoining Mozambique (Kröner et al., 2001). Previous age data suggest that Malawi experienced three phases of Precambrian tectonothermal activity: one at 3.5 Ga based on a K-Ar hornblende age (Ray et al., 1974); the Mesoproterozoic Kibaran metamorphic event implied by Rb-Sr ages obtained in southern Malawi (Andreolli, 1984; see also Pinna, 1993): and the later overprints by the Neoproterozoic Mozambique Belt event. Johnson et al. (2005) termed the region to have experienced the latter two components, the Southern Irumide Belt (SIB). However, high-precision zircon geochronology failed to confirm the existence of a Mesoproterozoic metamorphism in southern Malawi or in northern Mozambique (Muhongo et al., 2003; Kröner et al., 2001).

3. Sample Descriptions

Seventeen samples were collected for analysis, consisting of 7 variably foliated granites, 5 charnockitic gneisses, 3 gneisses, a syenite, and a massive granite. GPS coordinates for the analysed samples and a summary of U-Pb ages are given in Table 1. Fig. 2 shows location of the samples on a simplified geological map of southern Malawi.

The granites are buff to pink, variably foliated and coarsely crystalline. They occur in a belt about 30 km wide extending from the southeast of Mwanza (Fig. 2) in a north-westerly direction into Mozambique. Contacts between the granites and adjacent gneisses range from sharp and commonly sheared to gradational in which there is progressive decrease in foliation development over several metres. Fine grained mafic enclaves occur as oval shaped blebs with diffuse margins or angular bodies with sharp margins and are up to 30 centimetres in size. The granites contain 25-50% quartz, 10-25% plagioclase, and locally up to 20% K-feldspar. Mafic mineral phases include up to 20% hornblende, which in places replaces clinopyroxene, and 5-13% biotite. The main accessory phases are ilmenite and zircon.

The charnockitic gneisses occur in the Zomba, Blantyre and Mulanje mountain areas (Fig. 2) and were observed as alternating leucocratic, mesocratic and locally melanocratic bands. They are coarse, crystalline and foliated granulites and have been intruded by various phases of granites. In certain areas near Zomba, metasedimentary calc-silicates and limestones are interbanded with the charnockitic gneisses suggestive of a supracrustal origin. The charnockitic gneisses are absent in the western parts of the region where hornblende biotite gneisses dominate but due to poor exposure a clear and distinct contact could not be established between these two areas. Principal mineral phases in the charnockitic gneisses are up to 25% quartz, up to 40% plagioclase, up to 28% hypersthene and diopside, and up to 10% hornblende, with the latter locally replacing pyroxene. Accessory minerals include apatite, magnetite, and zircon.

Up to 30 m bands of quartzo-feldspathic gneiss occur concordant with the charnockitic gneiss. They consist of up to 55% quartz, generally equal amounts of plagioclase and microcline (15%) and 5% biotite with accessory zircon and opaque oxide minerals. One sample (#223A) contains up to 50% K-feldspar, along with 15% each of plagioclase and hornblende, 5% of biotite (5%) and about 20% quartz.

Syenitic to granitic intrusions occur in southern Malawi and two types have been defined. Older bodies in the north of Mwanza in what is called the Kirk Range area, around Chiradzulu, Blantyre, and close to Zomba (Fig. 2) are porphyroblastic, and vary from quartz-rich granitic gneisses to quartz-poor syenitic gneisses. Compositionally these contain up to 40% potassic feldspar, 35% perthitic feldspar, 5% plagioclase feldspar, 10% quartz, 5% biotite, 3% pyroxene, with accessories opaque oxide minerals and zircon. Until this study these bodies were radiometrically undated. The younger phase is the Upper Jurassic to Lower Cretaceous Chilwa Alkaline Province (Evans, 1965) of syenite and granite intrusions and includes the highest hills in the area, the Mulanje Mountain and Zomba Plateau (Fig. 2). They are unfoliated, buff to pink coloured, coarsely crystalline, and commonly contain a variety of mafic xenoliths. The outcrops include both syenitic and granitic rocks, possibly reflecting various intrusion phases, but no clear field contacts could be established to determine their relative age relationships. The rocks contain as much as 70% K-feldspar with plagioclase less than 5%. Quartz makes up 15% and hornblende and biotite each constitute up to 5% with accessory magnetite and zircon.

4. Analytical Methods

Representative granitoid and granitic gneiss samples from across southern Malawi were collected for zircon U-Pb and Hf, and whole rock Sm-Nd, isotopic measurement. Table 1 lists sample location and a summary of U-Pb results. Zircons for analysis were extracted by standard techniques, handpicked, mounted in epoxy resin, and polished to expose the grain centres. Backscatter electron (BSE) and cathodo-luminescence (CL) images of mounted zircon were acquired on an electron microprobe (JXA-8600 Superprobe) at the University of St Andrews, Scotland.

U-Pb zircon dating was carried out at the British Geological Survey Isotope Laboratory (NIGL) in Nottingham, UK, on an Attom single-collector ICP-MS (Nu Instruments, Wrexham, UK) coupled to a UP193SS Nd:YAG laser ablation system using a low-volume ablation cell. The carrier gas through the ablation cell was Helium and Ar make-up gas was connected via a Y-piece and obtained from a Nu Instruments DSN-100 desolvating nebulizer. On the SC-ICP-MS, masses ^{202}Hg, ^{204}Pb+Hg, ^{206}Pb, ^{207}Pb, ^{235}U were measured. The ^{238}U was calculated from ^{235}U using a ^{238}U/^{235}U of 137.818 (Hiess et al., 2012). Normalisations of the Pb/Pb and U/Pb ratios were carried out by bracketing primary reference material 91500, based on the average measured value of the reference material compared to the ratio determined by ID-TIMS (Wiedenbeck et al., 1995). The validation of accuracy of normalization was done by Standards GJ-1 and Plešovice (Jackson et al., 2004; Sláma et al., 2008) which also provided long-term variance statistics for uncertainty propagation (0.8 %/1.7 % 2s ^{207}Pb/^{206}Pb MC-ICP-MS/SC-ICP-MS respectively).

Analysis uncertainties represent measurement precision propagated with the excess variance of the reference material for the respective session. Age uncertainties are propagated for systematic components by quadratic addition and include the long-term variance of the reference materials on the ICP-MS, the uncertainties of the reference values as determined by ID-TIMS, and the decay constant uncertainties (e.g. Schoene et al., 2006). Total combined age uncertainties vary between 0.5-3 % (2 sigma; nb.: conversion of analysis uncertainty to age uncertainty is not linear; see Horstwood et al., 2016, and Spencer et al., 2016 for further discussion). Visualization of U-Pb Concordia and zircon ages is done using Isoplot v4.15 (Ludwig, 2003). Data were interpreted using the upper intercept ages or ^{206}Pb/^{238}U ages following Spencer et al. (2016).

Results of U-Pb and Pb-Pb analyses for reference materials during nine single collector sessions and twelve multi-collector sessions spanning six months are presented in Supplementary Data Table 1. Ratios for 91500 are self-normalized.

Non-ignited bulk rock samples were digested in HF-HNO3 to provide the solution for Sm - Nd analyses undertaken at NIGL. The concentration of light rare earth elements (LREEs) was determined using Eichrom AG50 cation exchange columns. Sm and Nd were loaded onto double-rhenium filament assemblies and analysed in multi-dynamic mode on a Thermo Scientific Triton thermal ionization mass spectrometer. $^{143}Nd/^{144}Nd$ is reported normalized to a preferred value of 0.512115 for the JNd-i standard (Tanaka et al., 2000). Measured $^{143}Nd/^{144}Nd$ ratios for the La Jolla standard are 0.512106 ± 0.000010 (2 sigma = 18 ppm, n = 15). Results for whole rock Sm-Nd isotopic analyses are presented in Supplementary Data Table 3.

Zircon ablation spots with near concordant (> 95 % concordance) U–Pb analyses from each of the samples were re-analysed for their Lu–Hf isotopic compositions. Isotope analyses were carried out at NIGL using a Thermo Scientific Neptune Plus MC-ICP-MS coupled to a New Wave Research UP193UC excimer laser ablation system and a TwoVol2 ablation cell. Helium was used as the carrier gas through the ablation cell with Ar makeup gas being connected via a T-piece and sourced from a Cetac Aridus II desolvating nebulizer. After initial set-up and tuning, the nebulizer was aspirating air during the ablation analyses. Masses ^{172}Yb, ^{173}Yb, ^{175}Lu, $^{176}Hf+Yb+Lu$, ^{177}Hf, ^{178}Hf, ^{179}Hf and ^{180}Hf were measured simultaneously using a 1 second integration time during a static, 30 second ablation analysis utilising a 35 μm diameter spot and a fluence of 8-10 J/cm^2 (see Spencer et al., 2014 for full methods). A standard–sample–standard bracketing technique, using fragments of Mudtank and 91500 as zircon reference materials, was employed to monitor accuracy and precision of internally corrected Hf isotope ratios and instrumental drift with respect to the Lu/Hf ratio. Hf reference solution JMC475 (both doped with 2 ppb Yb and undoped) was analysed during each analytical session to allow normalization of the laser ablation Hf isotope data. Correction for ^{176}Yb on the ^{176}Hf peak was made using a ^{176}Yb/^{173}Yb ratio calibrated for Hf mass bias using Yb-doped JMC475 solutions (cf. Nowell and Parrish, 2001). Additionally, Plešovice and Yb-doped synthetic zircon (Zr141 and Zr142; Fisher et al., 2010) were analysed to assess the accuracy of the Hf ratio normalization and Yb ratio correction, respectively. ^{176}Lu interference on the ^{176}Hf peak was corrected by using the measured ^{175}Lu and assuming ^{176}Lu/^{175}Lu = 0.02653. Systematic uncertainties of Hf and Lu isotope ratios were propagated using quadratic addition, incorporating the external variance of the reference material during each analytical session.

Results of Hf analyses over nine sessions spanning three weeks, for 91500, Mudtank, Plesovice, and Yb-doped synthetic zircon, are presented in Supplementary Data Table 2. Hf ratios of Mudtank are self-normalized. Two Yb-doped synthetic zircon containing varying amounts of Yb were also analysed. The lower Yb zircon (Zr141, Yb/Hf = ~0.08) yielded a precise and accurate arithmetic mean within uncertainty of the preferred value. The higher Yb zircon (Zr142, Yb/Hf = ~0.16) yielded a greater degree of scatter over the three-week period and returned > 200 ppm reproducibility within each daily session. Only 2 of the 341 sample analyses had Yb/Hf ratios beyond the range of Zr141 and even for these analyses the average Hf isotope ratio did not deviate from the range determined from the low Yb/Hf samples. It is therefore concluded that for this dataset the Yb/Hf isobaric interference is corrected accurately.

5. U-Pb Zircon Geochronology

Selected zircon Cathodoluminescence (CL) images for the samples are presented in Fig. 3. Full U-Pb analytical data for the samples are given in Supplementary Data Table 1.

Concordia plots of the samples are given in Fig. 4. Ages of igneous crystallisation range from Mesoproterozoic to Cretaceous, with the main phases of activity at the end of the Mesoproterozoic, the mid and late Neoproterozoic, and the Cretaceous. Early Palaeozoic metamorphic ages were recorded in the charnockitic gneisses. Weighted averages and corresponding mean squares weighted deviation (MSWD) are assessed for over- and under-dispersion using criteria visualized by Spencer et al., (2017) and uncertainties are reported as 2 standard deviations.

5.1 Foliated granite

The foliated granites range in age from 1128 ± 30 Ma to 531 ± 3.4 Ma. For sample BM 163, twenty-four grains were analysed. The zircons are transparent, yellowish, euhedral and prismatic, displaying oscillatory zoning and no inherited cores (Fig. 3a, b). Some grains display alternating darker and brighter zones in CL images with others having dark inclusions and overgrowths. Some are darker and featureless with no oscillatory zoning and these are considered metamorphic. The crystals are generally large, greater than 500 µm in length and 400 µm in width, with uranium (U) concentrations ranging from 17 to 284 ppm and Th concentrations ranging from 17-389 ppm. Th/U ratios range from 1.17 to 2.08. Seventeen spots have U concentrations <100 ppm and seven have >100 ppm. All twenty-four spots have Th/U ratios > 1. Eight analyses are concordant with a $^{207}Pb/^{206}Pb$ weighted average age of 1039 ± 12 (MSWD = 3.0; over-dispersion present). An upper intercept age of 1038.2 ± 6.8 Ma (MSWD = 1.2) (Fig. 4a) is indistinguishable from the $^{206}Pb/^{238}U$ age, which is interpreted as the age of emplacement of the sample..

In sample BM 174, zircons are euhedral, pyramidal and elongate displaying typical oscillatory zoning (Fig. 3c, d). Some have dark homogeneous cores enveloped by oscillatory-zoned brighter rims but overall are transparent, commonly showing dark inclusions. The zircons are >250 µm in width and up to 600 µm in length. Oscillatory zoning is interrupted in places by overgrowths and some zircons have suffered radiation damage. U concentrations range from 37-526 ppm and thorium from 40-380 ppm. The Th/U ratios range from 0.52 to 2.92. The oscillatory zoning and Th/U ratios indicate that these zircon grains are magmatic. Twelve concordant analyses from thirty-two analysed grains yielded a $^{207}Pb/^{206}Pb$ weighted mean average of 1029.3 ± 8.0 Ma (MSWD = 3.2; over-dispersion present). The upper intercept age of 1035.6 ± 8.3 Ma (MSWD 1.2) (Fig. 4b) is interpreted as the age of crystallisation and is indistinguishable from the weighted average $^{207}Pb/^{206}Pb$ age.

For sample BM 179, zircons are relatively large (>200 µm wide and >600 µm in length) with some dark inclusions, euhedral and prismatic in shape, and display characteristic oscillatory zoning (Fig. 3e, f). Some of the zircons have a featureless darker core, which is clearly inherited and mantled by an oscillatory-zoned phase. Twenty-four grains were analysed. Eight were concordant but one (#179_22a) has higher uranium and thorium counts than the others and yields a lower $^{207}Pb/^{206}Pb$ age, which we interpret as a result of Pb loss and omit this age from our age calculations. The $^{207}Pb/^{206}Pb$ weighted average for the other seven grains is 1047 ± 12 Ma, MSWD = 1.4). The upper intercept age is 1047 ± 13 Ma (MSWD = 1.0) (Fig. 4c) and this is interpreted as the age of crystallisation of the sample.

Twenty-four grains were analyzed from sample BM 209. The zircons are mostly transparent, but some are dull brown, and range between >200 µm - 250 µm in width and >250 µm - 600 µm in length; they show euhedral and pyramidal shapes with oscillatory zoning, have dark inclusions and some crystals show radiation damage (Fig. 3 g, h). The U concentrations for the concordant spots range from 74-151 ppm whilst Th ranges from 32-107 ppm. The Th/U ratios are from 0.39-0.71. Twenty-four analyses were obtained of which eight were concordant and yielded a $^{207}Pb/^{206}Pb$ weighted average age of 1023 ± 21 Ma (MSWD = 5.5; over-dispersion present). The analyses yielded an upper intercept age of 1040 ± 25 Ma

(MSWD = 2.1) (Fig. 4d) and because this has a lower MSWD compared to the weighted average age, this is interpreted as the crystallisation age for the granite.

Zircons from foliated granite sample BM 213G are euhedral and pyramidal with widths >250 μm - 400 μm and the lengths typically >250 μm - 600 μm. They show oscillatory zoning and some display inherited cores (Fig. 3 i, j). Dark inclusions are present and some grains show evidence of radiation damage. U concentrations range from 73-393 ppm whilst Th ranges from 32 to 187 ppm. The Th/U ratios range from 0.36-0.69. Of twenty-five analysed grains, only one spot, which is from the rim was concordant (#213G_23) and yielded a ^{207}Pb/^{206}/Pb age of 1035 ± 21 Ma, which is interpreted as the age of emplacement. The analyses yielded an upper intercept age of 1088 ± 23 Ma (MSWD = 1.5) (Fig. 4e) that is interpreted as the age of inheritance. It must, however, be noted that the discordant ages are both from the rims and cores.

Zircons from foliated granite BM 256 are euhedral, pyramidal, and in range between 300 μm - 400 μm in width and up to 600 μm in length (Fig. 3 m, n). They display oscillatory zoning with some crystals showing darker overgrowths. Radiation damage is evident in some grains and some have dark inclusions. U concentrations range from 106 to 1649 ppm and Th ranges from 52 to 2297 ppm. The Th/U ratios range from 0.37 to 1.39. Of the seventeen analyses from sample BM 256 only four were concordant and yielded a ^{207}Pb/^{206}Pb weighted average age of 1033 ± 40 (MSWD = 7.5; over-dispersion present) interpreted as the age of emplacement. All analyses yielded an upper intercept age of 1070 ± 16 Ma (MSWD = 1.0) (Fig. 4g), which may be interpreted to reflect the age of an inherited component within the source.

Sample BM 213X is a fine- to medium-crystalline, mesocratic mafic enclave in metagranite sample BM 213G. Zircons are subhedral and pyramidal, with widths of 200 μm and lengths typically >250 μm - 400 μm. They show dark inclusions and appear damaged.

Some crystals show inherited cores with oscillatory zoning (Fig. 3 k, l). U concentrations for the concordant spots range from 86-430 ppm whilst Th ranges from 39 to 315 ppm. The Th/U ratios range from 0.42-0.79. Twenty-four analyses were obtained of which twelve were concordant. The $^{207}Pb/^{206}Pb$ weighted average for the concordant grains is 1023 ± 15 Ma, (MSWD = 5.5; over-dispersion present). The analyses yielded an upper intercept age of 1034 ± 17 Ma (MSWD = 1.1) (Fig. 4f), which is interpreted as the crystallisation age and is coeval with the hosting granite sample BM 213G. As in sample BM 213G, discordant ages were obtained from both the rims and cores.

5.2 Charnockitic Gneiss

Sample BM 249 is a mesocratic to leucocratic, coarse grained, charnockitic gneiss with perthitised plagioclase feldspar (14%), quartz showing wavy extinction (54%), clino and ortho-pyroxenes (12%) and biotite (20%). Accessory minerals include zircon, ilmenite and magnetite. Different varieties of zircons were recovered from Sample BM 249. Some are euhedral with oscillatory zoning and dark inclusions whilst others display a featureless darker core, a brighter mantle with oscillatory zoning, and a bright thin rim. These are interpreted as magmatic but with inherited cores (Fig. 3 o, p). The other group are dark and featureless showing no cores or mantles, have euhedral to subhedral shapes, sometimes pyramidal with rounded edges, and are interpreted as metamorphic. All the zircons have suffered radiation damage and contain dark inclusions with some crystals displaying variable overgrowths. In width, the zircons range from 250 µm to ~400 µm and in length they are up to 600 µm. U concentrations range from 97-332 ppm and Th ranges from 39-266 ppm and the Th/U ratios range from 0.33-0.80. 26 zircon grains were analysed with fourteen concordant. The weighted average $^{207}Pb/^{206}Pb$ age for the fourteen grains is 1027 ± 11 (MSWD = 4.8; over-dispersion present). The analyses yield an upper intercept age of 1036 ± 15 Ma (MSWD =

2.0) (Fig. 4h) and this is indistinguishable from the weighted average age within error and is therefore interpreted as the crystallisation age of the charnockitic gneiss.

Sample BM 252 is a leucocratic, coarse grained, foliated charnockitic gneiss. The rock comprises quartz (43%), plagioclase feldspar (34%), pyroxenes (14%), hornblende (5%), and accessory zircons and magnetite. Only three zircon grains were recovered from BM 252 and this was consistent with relatively low Zr content determined in XRF analyses. One grain showed oscillatory zoning under CL whereas the other two are bright, featureless with some dark inclusions, and with rounded edges, which we interpret as metamorphic (Fig. 3 q, r). Eight analyses within the inferred magmatic grain (#252-2a, 2b, 2c, 2d, 2e, 2f, 2g, 2h) had Th/U ratios range from 0.32-0.44. Six spots yielded discordant ages. The two concordant spots (#252-2a and #252-2c) yielded a weighted average $^{207}Pb/^{206}Pb$ age of 1089 ± 160 Ma. Although the error is large, this is interpreted to approximate the age of emplacement of the charnockite. An alternative interpretation is that the older age (1102 ± 21 Ma) represents the actual emplacement age and the younger age (1077 ± 20 Ma) may be an age affected by Pb loss. However, such an interpretation needs caution as the two spots are from the same rim. Thirteen spots were analysed from the other two zircon grains that had Th/U ratios of 0.01 to 0.40. The spots analyses yielded dates < 600 Ma. Eight of the thirteen analyses were concordant and yielded a weighted average $^{206}Pb/^{238}U$ age of 535.9 ± 6.7 Ma (MSWD = 0.6) and this is interpreted as the age of high grade metamorphism. The upper intercept age for the data set from the three grains is 1128 ± 30 Ma and the lower intercept age is 515 ± 18 Ma (MSWD = 1.1) (Fig 4i), consistent with the CL data and age groupings of the three grains being related crystallisation and metamorphism of the charnockitic gneiss.

Sample 281 is a mesocratic, coarse grained charnockitic gneiss composed of plagioclase feldspar (42%), quartz (12.0%), k-feldspar (9%), and ortho and clinopyroxene (28%), biotite (8%). Accessories include zircon and apatite. Seven zircon grains were separated from sample BM 281 and are anhedral/subhedral and somewhat prismatic with dark inclusions. Two did not luminesce and are therefore dark in CL. Four grains have dark cores, surrounded by oscillatory-zoned rims. They display rounded terminations in the pyramids and are likely metamorphic zircon. One zircon grain shows regular oscillatory zoning with a euhedral pyramidal shape and is interpreted as magmatic. Zircon grains range from 250 µm - 400 µm in width and from 300 µm to 600 µm length. U concentrations range from 117 to 2379 ppm, and are recorded with Th concentrations ranging from 3 to 216 ppm. In three analyses, the U concentrations were 600-2379 ppm. The Th/U ratios range from 0.02-0.84. For this group of zircons, two concordant populations are displayed (see Fig. 4j). The first population is around 600 Ma and these spots are from oscillatory zoned rims of zircon (#281-7) and they give an upper intercept age of 594 ± 65 Ma (MSWD = 1.4) but the lower intercept does not correspond to any known geological event. We interpret this date as the emplacement date of the protolith. The second population is around 500 Ma and these are from the other four zircon grains and rims. The weighted average $^{206}Pb/^{238}U$ age for this population is 493 +/- 22 Ma (MSWD = 0.12) and the date is interpreted as the time of metamorphism.

Sample BM 282A is leucocratic to mesocratic, medium to coarse grained charnockitic gneiss with a banded foliation in outcrop. It comprises plagioclase feldspar (39%), quartz (19%), K-feldspar (20.0%), hornblende (10%), diopside (5%), orthopyroxene (3%), and biotite (1%). Accessory minerals include zircon, ilmenite, apatite and magnetite. Thirty-one analyses were obtained from 3 grains from BM 282A. Six analyses yielded ages >1000 Ma, fifteen gave ages <745 Ma, and fifteen were discordant. Of the six with ages >1000 Ma five are from oscillatory zoned zircon cores and have Th/U ratios from 0.35-0.55. Analysis spot #282A-32 from these six is concordant and yielded a $^{207}Pb/^{206}Pb$ age 1075 ± 27 Ma and this is interpreted as the age of protolith emplacement. Fifteen spots with ages <745 Ma were concordant and yielded a $^{206}Pb/^{238}U$ weighted average age of 581 ± 20 Ma (MSWD = 14; over-dispersion present). This is interpreted as reflecting new zircon growth during regional metamorphism. The upper intercept age is 1187 ± 53 Ma and the lower intercept is 536 ± 24 Ma (MSWD = 3.7; over-dispersion present) (Fig. 4k).

Sample BM 282B is a leucocratic, medium to coarse grained, well foliated charnockitic granulite. It occurs interbanded with the mesocratic charnockitic gneiss (Sample BM 282A) and comprises plagioclase feldspar (50%), quartz (32%), pyroxene (7%), and accessory magnetite and zircon. Eighteen analyses were obtained from seven zircon grains from sample BM 282B and fourteen were concordant yielding ages <715 Ma. One grain yielded an age of 715 ± 18 Ma which is interpreted as emplacement age of protolith. The remaining thirteen analyses fall along Concordia between ca. 580 and 500 Ma (Fig. 4 p). The rounded termination of zircon crystals implies they are metamorphic. The ages may indicate either a growth of zircon at 580 ca. Ma during a metamorphic event with subsequent Pb loss at ca 500 Ma or, conversely, two distinct metamorphic events.

5.3 Remaining rock types

Sample BM 200 is a leucocratic, fine to medium grained foliated quartzo-feldspathic gneiss. Recovered zircons are non-luminescent and metamict. The backscatter (BSE) images reveal euhedral, pyramidal shapes with brighter cores that have abundant dark inclusions. The rims are darker with abundant fracturing and less inclusions than the cores. U concentrations range from 73-1820 ppm (average 849 ppm) and Th concentrations range from 18-171 ppm. The Th/U ratios are from 0.10-0.90. These are xenocrystic zircons with the likelihood that the high U concentrations in the core generated radiation damage that is responsible for the fracturing of the rim (Corfu et al., 2003). Of the thirty-five analyses obtained, seven were concordant of which four are >900 Ma with a $^{207}Pb/^{206}Pb$ weighted average age of 1031 ± 34

Ma (MSWD = 4.0; over-dispersion present). The other three concordant grains yield a $^{206}Pb/^{238}U$ weighted average age of 607 ± 41 Ma (MSWD = 5.0; over-dispersion present). The data set (Fig. 4m) is difficult to interpret but the Mesoproterozoic age is similar to the metagranites and may represent magmatism at this time, whereas the Neoproterozoic age may reflect partial or complete resetting during subsequent metamorphism.

Sample BM 221 is foliated leucogranite gneiss. Twenty-two analyses were undertaken on four zircon grains with the three most concordant grains yielding a $^{206}Pb/^{238}U$ weighted average age of 735 ± 69 Ma (MSWD = 0.24). The concordant grains were oscillatory zoned with a Th/U ratio of 0.53 and their weighted average age is interpreted as the age of crystallisation of the sample. The upper intercept age for the data set is 764 ± 20 (MSWD = 13; over-dispersion present) (Fig. 4 n) interpreted to reflect the age of an inherited component within the source.

Sample 223A is a medium grained, buff to pink coloured gneiss. The rock comprises K-feldspar (60%), quartz (17%), plagioclase feldspar (15%) hornblende (17%) and biotite (5%). Zircon and magnetite are accessory phases. Only two zircon crystals were recovered resulting from poor separation. Five zircon analyses were obtained, four of them concordant. Three concordant analyses from oscillatory zoned parts of the grains yielded a weighted average $^{207}Pb/^{206}Pb$ age of 956 ± 12 Ma (MSWD = 0.93) interpreted as the crystallisation of age of the leucogranite. The other grain analysis yielded a date of 541 ± 17 Ma. The five analyses yielded an upper intercept age of 969 ± 53 Ma and a lower intercept of 589 ± 42 Ma (MSWD = 0.1) (Fig. 4 o). The gneiss protolith is thus inferred to have crystallized at 969 ± 53 Ma, which is indistinguishable within error to the weighted average $^{207}Pb/^{206}Pb$ age. The sample underwent Pb loss in a subsequent metamorphic event at 589 ± 42 Ma.

Sample BM 289 is a leucocratic, medium- to coarse-grained foliated perthitic syenite. The rock is porphyroblastic comprising 40% potassic feldspar, 36% perthitic feldspar, 5%

plagioclase feldspar, 8% quartz, 5% biotite, 3% pyroxene, with accessories of unknown opaque minerals. Zircons show euhedral, pyramidal shapes, and oscillatory zoning and are considered to be magmatic. Others exhibit alternating darker and brighter phases with the latter phases having oscillatory zoning and the former being featureless. These are interpreted to be inherited zircons overgrown by metamorphic phases. U concentrations are from 19-435 ppm whilst Th ranges from 45-621 ppm. The Th/U ratios range from 0.29-2.40. Of the twenty-one analyses of oscillatory zoned zircon, seventeen were concordant with a weighted average $^{206}Pb/^{238}U$ age of 531 ± 3 Ma (MSWD = 0.5) Fig. 4i) was obtained which is interpreted as a crystallisation age of the syenite.

Sample BM 240 is a brown to pink, coarse grained, massive, homogeneous K-feldspar rich granite. Subhedral to anhedral quartz makes up about 13%. Minor amounts of hornblende occur and are characterized by distinctive pleochroism (in shades of green) and euhedral/subhedral crystals. Pleochroic euhedral elongated biotite crystals make up c. 4% and are subordinate to hornblende. Magnetite is the predominate accessory mineral. The twenty analysed oscillatory zoned grains have Th/U ratios of 0.53-1.15. They fall into three age groups along Concordia at 155 ± 6 Ma (n = 2), 141 ± 6 Ma (n = 1), and 124 ± 5 Ma (n = 18) (Fig. 4 q). The youngest age group is considered to be the time of zircon crystallisation with the two older ages representing inherited grains.

6. Sm-Nd Isotopes

Results for whole rock Sm-Nd isotopic analyses on granitoids from Southern Malawi are presented in Supplementary Data Table 3. Neodymium epsilon (εNd_T) values are calculated at magmatic crystallisation ages as determined by U-Pb dating for each sample. Samples with $^{147}Sm/^{144}Nd > 0.165$ are considered to yield unreliable model ages (Stern, 2002). All the samples in this study have $^{147}Sm/^{144}Nd < 0.16$ except for sample BM 252. The whole rock Sm-Nd data show elemental quantities of Sm ranging from 0.9 to 33 ppm and Nd ranges from 5.4 to 154 ppm. The $^{147}Sm/^{144}Nd$ ratios range from 0.0986 to 0.1814 and ratios for $^{143}Nd/^{144}Nd$ range from 0.512104 to 0.512811. Calculated TDM model ages range from 1153 to 1801 Ma with the mean at 1535 Ma. The εNd_0 values are all negative and have a wide range from -10.3 to -2.2. The εNd_T values range from -5.0 to +5.8 suggestive of substantial contributions to the crust from radiogenically depleted sources with some contributions from enriched continental sources. Model ages range from late Paleoproterozoic to late Mesoproterozoic (ca 1.8 Ga to 1.1 Ga).

Sm-Nd isotopic data on granitoids from Malawi have been utilised to calculate εNd_T, which are plotted on Fig. 5, and include data presented herein as well as that of Kröner et al. (2001). Five of the metagranites (BM 163, BM 174, BM 179, BM 209 and BM 213G) have U-Pb ages between 1047 and 1033 Ma and have crustal model ages of 1613 Ma to 1442 Ma and εNd_T from +1.7 to +3.6. The data suggest derivation of these granites from a slightly depleted source that separated from the mantle at around 1500 Ma and was then remobilised at around 1040 Ma. The foliated granite enclave BM 213X shares these characteristics but with a slightly older crustal model age of 1638 Ma. One foliated granite (BM 256) has a slightly older U-Pb age of 1070 Ma and a model age of 1681 Ma.

Three charnockitic gneisses, BM 249, BM 281 and BM 282A, yielded discrete U-Pb ages of ca. 1036, 592 and 540 Ma, respectively, indicating separate thermal events. Their crustal model ages are 1642, 1700 and 1611 Ma, respectively, and show some variation in their εNd_T values, +1.4, -4.5 and +0.7, respectively. Thus, the sources of the charnockitic gneisses vary from enriched mantle or crustal remelts to slightly depleted mantle, and that they likely separated from the mantle at around 1650 ± 50 Ma.

Three gneisses, a syenite and an unfoliated granite have very different U-Pb ages, and provide a range of Nd isotopic data. Quartzo-feldspathic gneiss BM 200 has a U-Pb age of

1031 Ma with an initial εNdT value of +5.8 and a crustal model age of 1568 Ma. These characteristics are similar to several foliated granites and a charnockitic gneiss enabling placing BM 200 into that magmatic episode. Leucocratic gneiss (BM 223A) yields a U-Pb age of 956 Ma, εNdT value of +1.6 and a crustal model age of 1426 Ma. These characteristics do not match any of the other samples and appear to represent a discrete event. A foliated hornblende-, biotite-bearing gneiss (BM 221) has a U–Pb age of 756 Ma, an initial εNdT value of +2.5, and a crustal model age of 1153 Ma. This also appears to represent a separate event. The two anomalous dates however, may be a result of error arising from Pb-loss or inheritance and/or disturbance of the isotope systematics and there is need to carry out further investigations to arrive at certain conclusions.

A foliated perthitic syenite (BM 289) gives a U–Pb age of 531 Ma, an initial εNdT value of -5.0 and a crustal model age of 1801 Ma, and this also appears to be a unique event. Finally, a very young event likely associated with the East African Rift is represented by an unfoliated granite (BM 240) with a U–Pb age of 124 ± 5 Ma, an initial εNdT value of -3.4 and a crustal model age of 1497 Ma. This group of diverse samples appear to represent different events, at least based on U-Pb ages and Nd isotope systematics, with one coinciding with the main group of foliated granites.

7. Hf isotopic analyses

Hf analyses were performed on zircon grains from 7 foliated granite samples, three charnockitic gneisses, a quartzo-feldspathic gneiss, a leucogranite, a massive granite, and a hornblende biotite gneiss. See Supplementary Data Table 2 for further information.

7.1. Foliated granites and charnockitic gneisses

Hf spot analyses were carried out on selected zircons from the foliated granites and charnockitic gneisses and their results are summarized in Table 2. The analyses yielded initial εHf$_T$ values of +3.8 to +9.2 with a mean εHf$_T$ of +6.3. The corresponding two-stage depleted mantle model ages (TDM) range from 1335 to 1952 Ma. The overall positive εHf$_T$ values for the foliated granites and charnockitic gneisses suggest derivation from isotopically depleted source akin to the depleted mantle. Notwithstanding the few samples that have negative εHft values suggesting derivation from crustal melts.

7.3 Other Rock Types

Fifteen Hf spot analyses were carried out on two populations of concordant grains from quartzo-feldspathic gneiss BM 200. The older population corresponding to age of igneous crystallisation at 1031 ± 34 Ma yielded initial εHf$_T$ values of +7.7 to +10.3 and TDM ages from 1761 to 1443 Ma. The positive initial εHft values signify derivation from depleted mantle during the early Proterozoic. The younger population analyses with a mean U-Pb age of 607 ± 41 Ma which is interpreted to represent emplacement yielded initial εHf$_T$ values of -3.5 to +2.5 and TDM ages of 929 Ma. The negative initial εHft values suggest derivation from enriched mantle.

BM 221 is a hornblende, biotite-bearing gneiss and two Hf spot analyses were carried out on concordant grains which yielded initial εHf$_T$ values of +4.3 and +4.6 and corresponding TDM ages range from 1599 Ma and 1585 Ma. From leucogranite BM 223A, four Hf spot analyses were carried out on concordant grains and they yielded initial εHf$_T$ values of +5.5 to +8.1 and TDM ages that range from 1813 to 1670 Ma. The positive εHft values for these two samples suggest derivation from isotopically depleted source i.e. depleted mantle.

Seven Hf spot analyses were carried out on concordant zircon grains from perthitic syenite sample BM 289. They yielded initial εHf$_T$ values from -2.7 to + 1.4 and TDM ages range from 1496 to 1742 Ma. The presence of negative εHf$_T$ suggests origins from more evolved crustal material.

Seven Hf spot analyses were carried out on concordant grains from granitoid BM 240 (124 Ma) yielding initial εHf$_T$ values of -7.2 and -3.8 and depleted mantle model ages (TDM) range from 1479 to 1293 Ma. The negative εHf$_T$ suggest therefore derivation from crustal material.

In summary the gneisses, perthitic syenite and granite in this group exhibit a wide range of initial εHfT values (- 7.2 - +10.3) suggesting that the rocks represent mixtures of mantle derived melts and crustal derived melts.

8. Crustal Evolution of Southern Malawi

A εHf$_T$ vs U-Pb age evolution diagram for the southern Malawi granitoids is presented in Fig. 5. εHf$_T$ values fall into four major age populations in the Mesoproterozoic (~1040 Ma), Neoproterozoic (~760 Ma), Cambrian (~530), and the Jurassic (~120). An important relationship shown by this diagram is the steep reworking trend in the data with a ^{176}Lu/^{177}Hf ratio of 0.015 projecting back to an average model age of ~1.5 Ga. This implies not only that the continental crust in southern Malawi can broadly be attributed to a single crustal reservoir, but that the initial isotopic composition has not changed dramatically beyond the average continental crust (^{176}Lu/^{177}Hf ratio of 0.015; Griffin et al., 2004).

9. DISCUSSION

U-Pb, Sm-Nd and Lu-Hf isotopic data for granitoid rocks from southern Malawi provide constraints on the timing and sources of magmatic activity within the Malawian segment of the Mozambique Belt and its role in Rodinia and Gondwana supercontinent cycles. U-Pb data indicate the region preserves a record of Mesoproterozoic, Neoproterozoic, Cambrian, and Cretaceous igneous activity. The samples display no evidence for the presence of late Archean reworked crustal precursors that have been suggested by Andreolli (1984) and found in neighbouring regions (Thomas et al., 2016a).

9.1 Magmatism

Magmatism during the Mesoproterozoic spanned a hundred million years and occurred in three pulses at ca. 1130 Ma, 1070 Ma, and 1050 to 1030 Ma. The oldest magmatic event in the study region (1128 ± 30 Ma) corresponds with the emplacement of a charnockitic gneiss (sample BM 252) occurring southwest of Mulanje. All the foliated granite samples have Mesoproterozoic emplacement ages. The emplacement of the protolith of the hornblende biotite gneiss occurred ~956 Ma, with a leucogranite intruding at ca. 756 Ma and charnockitic gneiss sample BM 281 intruded later, at ca. 600 Ma. Emplacement of a perthitic syenite at Chiradzulu Hill to the north of Blantyre occurred at ~594 Ma.

The youngest magmatism is dated as Cretaceous at 124 ± 5 Ma. The sample is from Mulanje Mountain, which falls within the Chilwa Alkaline Province that defines a strong pulse of magmatism associated with the East African rift system ranging from 135 to 105 Ma (Woolley et al., 1987).

9.2 Metamorphism

Metamorphism has been dated from charnockitic gneiss sample BM 252 that yielded a lower intercept age of 515 ± 18 Ma. Occurrence of featureless zircons with rounded terminations was noted in sample BM 252 (Fig. 3 q) with weighted average $^{206}Pb/^{238}U$ age of 535.9 ± 6.7 Ma (MSWD = 0.6). The metamorphic age is consistent with a monazite $^{207}Pb/^{235}U$ age of 522 ± 17 Ma for amphibolite metamorphism of Neoproterozoic nepheline gneisses in southern Malawi (Ashwal et al., 2007), but younger than peak regional granulite facies metamorphism in the central part of Tanzania, which is dated at c 640 Ma (Sommer et al., 2003). Sample BM 200 yielded in a second population a younger U-Pb age date of 607 ± 41 Ma. This is interpreted as complete or partial resetting in the zircon during a possible metamorphic event, implying metamorphism could have started much earlier i.e. peak regional granulite facies metamorphism in the central part of Tanzania has been dated at c 640 Ma (Sommer et al., 2003). The age of metamorphism in the Southern Irumide Belt is dated ca. 615 – 517 Ma (Johnson et al., 2005), the oldest ages coming from the Lurio Nampula Belts. The lower intercept ages in the Concordia for the foliated granites and charnockitic gneisses though with large error margins are basically Cambrian (ca 536 Ma or less) implying some Pb loss event(s) likely linked to collisional events associated with Gondwana assembly.

9.3 Geotectonic setting and sources of magmatism

Radiogenic isotope data in the Mesoproterozoic rock samples show positive εNd and εHf values signifying limited contribution from depleted mantle material, whereas rocks with younger emplacement ages display negative epsilon values suggestive of crustal material recycling and mixing for their source and origins (Fig. 5). The temporal evolution of εHf_T as constrained by U-Pb zircon ages indicates crustal reworking with time, with the youngest granitoids (~535-515 Ma) being essentially crustal melts.

U-Pb age data from Malawi are plotted on a time-space diagram (Fig. 6) alongside data from the Southern Irumide Belt (SIB) to the west of Malawi in Mozambique and Zambia (Johnson et al., 2005), the Mozambique Belt in Tanzania (Sommer et al., 2003), and the Mozambique Belt in Mozambique (Bingen et al., 2009). There are no data for magmatic events in southern Malawi pre- 1100 Ma and the overall age pattern is similar to the Mozambique Belt in Mozambique where magmatism is no older than 1200 Ma. The data from neighbouring Southern Irumide Belt shows magmatism between 1450 Ma and 950 Ma and none in the Paleoproterozoic and Archean periods (Macey et al., 2010; Thomas et al., 2016b). A weakly deformed Murrupula Suite porphyritic quartz monzonite in the Nampula complex in Mozambique returned a crystallization age of 533 ± 5 Ma, and undeformed Murrupula Suite granites yielded ages between 525 and 495 Ma (Macey et al., 2010). The data from Tanzania contrasts with that in Malawi, Mozambique and Southern Irumide Belt, and shows magmatism is dominantly in the Paleoproterozoic and Archean.

The time-space plot (Fig. 6) shows the timing of magmatism and metamorphism based on available U-Pb age data. The Mozambique Belt in Malawi, Mozambique and Tanzania shows evidence for Neoproterozoic (Pan-African) magmatism and metamorphism but none from the Southern Irumide Belt. However, data is available showing magmatic activity at c. 740, 650, and 540 from lithologies in the South Irumide Belt of Zambia region that were deformed during Gondwana amalgamation (Johnson et al., (2006). Hanson (2003) stated that arc-type lithologies overlying both the Malawi and Mozambique regions are overprinted by the Pan-African event but questioned if they were derived from a continuous Mesoproterozoic crust that was present in the region prior to the Pan African event, or were minor crustal slices or terranes accreted during collisional assembly of the Mozambique Belt. Our data lends more credence to the former supposition and it is suggested therefore, that the lithologies of the Southern Irumide Belt in Zambia continue into southern Malawi and Mozambique.

Geochemical data on the late Mesoproterozoic to early Neoproterozoic magmatic activity in the Mozambique Belt (Bingen et al., 2009; Grantham et al., 2003), suggest formation in a convergent plate margin setting. This is substantiated by the ^{176}Lu/^{177}Hf trajectory of the zircon Hf data presented herein that approximate the expected trajectory of average continental crust (~0.015; Griffin et al., 2002). This time period corresponds with Rodinia assembly (e.g. Li et al., 2008) however, there is no unequivocal evidence for Rodinia-age collisional orogenesis in southern Malawi. This is consistent with other orogenic belts of a similar age on the African continent from the Namaqua-Natal belt in southern Africa (Eglington et al., 2003; Jacobs et al., 2008; Spencer et al., 2014; Thomas et al., 2016a), Irumide Belt (de Waele et al., 2009), and Southern Irumide Belt (Thomas et al., 2010; Hauzenberger et al., 2014; Thomas et al., 2016b). As with other Rodinia-age orogenic belts in sub-Saharan Africa, the lack of clear evidence for collisional orogenesis argues for either an exterior subduction system or a highly oblique collisional orogeny. Magmatism in the Neoproterozoic i.e. 756 Ma in southern Malawi has been attributed to events related to Rodinia breakup (Ashwal et al., 2007), although the spatial relationships between these southern Malawi events and those of other Rodinia blocks could not be ascertained. The perthitic syenite BM 289 yielded a crystallisation age of 531 ± 3.4 Ma, similar to ages in the region associated with reactivated rifting (Bloomfield, 1965; Evans, 1965; Garson et al., 1965). Cambrian (ca 520-510 Ma) metamorphism reported in this study and Ashwal et al. (2007) corresponds with the timing of collisional events associated with Gondwana assembly. Differences between southern Malawi and Tanzania and Mozambique in the timing of metamorphism in the Mozambique Belt suggest a complex history of continental thickening and exhumation.

Lastly, the Cretaceous granitoid (BM 240) likely associated with the East African Rift does not show any indication of mantle influence despite this being the case for most magmatism associated with the rift system (Furman and Graham, 1999). These data may further imply that what was previously thought to be heterogeneities in the mantle (Norry et al., 1980) can more simply be associated with assimilation of continental crust.

10. CONCLUSION

Zircons from granitoids in southern Malawi have emplacement ages ranging from late Mesoproterozoic to Cambrian (1128 Ma – 531 Ma) and model ages from late Paleoproterozoic to early Mesoproterozoic (1952 Ma – 1335 Ma). The lower intercept zircon $^{206}Pb/^{238}U$ age of 515 ± 18 Ma from charnockitic gneiss BM 252 is interpreted as the time of metamorphism and deformation associated with collisional and suturing events during the assembly of East and West Gondwana. Our radiogenic isotope (Sm-Nd) and the Lu-Hf data suggest that the source of magmatism can be ascribed to a single crustal reservoir first extracted from the mantle (1952 Ma). Subsequent magmatic events simply reworked this pre-existing crust.

The absence of isotopic evidence of Archean magmatism and reworking in the studied lithologic units would suggest that all the magmatic and metamorphic events are related to igneous and tectono-thermal events resulting from crustal thickening in a collisional environment (Muhongo et al., 1994) with the exception of the Cretaceous, East African Rift related sample.

Our study of the amphibolite- to granulite-facies granitoids in southern Malawi found no evidence for Mesoproterozoic metamorphism and supports previous studies which suggest Mesoproterozoic to Neoproterozoic magmatism was overprinted by later Neoproterozoic-Cambrian metamorphism.

ACKNOWLEDGEMENTS

First author would like to thank the University of Malawi (Chancellor College) and the University of St Andrews for sponsorship to study for a PhD through which the field research data was generated. U–Pb zircon geochronology and Nd isotope analyses at (NIGL) were supported by NERC grant NIGF- IP-1453-0514 to Cawood and Manda. Peter Cawood acknowledges support from Australian Research Council grant FL160100168. The manuscript also greatly benefitted from two anonymous reviewers.

FIGURE CAPTIONS

Fig. 1: Map showing the probable position of Malawi during Gondwana assembly (after Spencer et al., 2013).

Fig. 2: Map showing simplified regional geology of southern Malawi and sample locations of this study.

Fig. 3: Cathodoluminescence Images (CL) for zircons from selected foliated granites and charnockitic gneisses from southern Malawi.

Fig. 4: U-Pb Concordia diagrams of samples from this study.

Fig. 5: a) εNd_t versus U-Pb age (Ma) plot for granitoids from southern Malawi. b) εHf_t versus U-Pb age (Ma) plot. $^{176}Lu/^{177}Hf$ ratio of 0.015 represents the average crustal evolution trajectory of average continental crust (Griffin et al., 2004).

Fig. 6: Time-space plot for tectonothermal events in Malawi, Southern Irumide Belt (SIB), Tanzania, Mozambique, and Antarctica. See text for references.

11. REFERENCES

Andreolli, M. A. G., 1984, Petrochemistry, Tectonic Evolution and Metasomatic Mineralizations of Mozambique Belt Granulites from S Malawi and Tete (Mozambique), Precambrian Research, Volume 25, Issue 1-3, pp. 161-186.

Andersen T., Griffin W. L. & Pearson N. J., 2002, Crustal Evolution in the SW Part of the Baltic Shield: the Hf Isotope Evidence, Journal of Petrology (2002) 43 (9): 1725-1747. doi: 10.1093/petrology/43.9.1725

Ashwal L. D., Armstrong R. A., Roberts R. J., Schmitz M. D., Corfu F., Hetherington C. J., Burke K., Gerber M., 2007, Geochronology of Zircon Megacrysts from Nepheline-bearing

Gneisses as Constraints on Tectonic Setting: Implications for Resetting of the U-Pb and Lu-Hf Isotopic Systems, Contributions to Mineralogy and Petrology (2007) 153:389–403, DOI 10.1007/s00410-006-0153-

Bingen, B., J. Jacobs, et al., 2009, "Geochronology of the Precambrian Crust in the Mozambique Belt in NE Mozambique, and Implications for Gondwana Assembly." Precambrian Research 170(3–4): 231-255.

Bloomfield, K. 1965, The Geology of the Kirk Range-Lisungwe Valley Area, Bulletin 7, Geological Survey Department, Malawi, Government Printer, Zomba, Malawi.

Bloomfield, K. 1970, The Geology of the Zomba Area, Bulletin 16, Geological Survey of Malawi, Government Printer, Zomba, Malawi.

Cawood P. A. & Buchan C. 2007, Linking accretionary orogenesis with supercontinent assembly, Earth-Science Reviews, Volume 82, Issues 3–4, June 2007, Pages 217–256

Collins, A. S. and Pisarevsky S. A., 2005, "Amalgamating eastern Gondwana: The evolution of the Circum-Indian Orogens." Earth-Science Reviews 71(3–4): 229-270.

Daly, M. C., 1986, "The intracratonic Irumide Belt of Zambia and its bearing on collision orogeny during the Proterozoic of Africa." Geological Society, London, Special Publications 19(1): 321-328

De Waele B., Fitzsimons I. C. W., Wingate M. T. D., Tembo F., Mapani B., and Belousova E. A., 2009, The Geochronological Framework of the Irumide Belt: A Prolonged Crustal History Along the Margin of the Bangweulu Craton, American Journal of Science, Volume 309, February, 2009, Page 132–187, DOI 10.2475/02.2009.03

Eglington, B.M., Armstrong, R.A., 2003. Geochronological and isotopic constraints on the Mesoproterozoic Namaqua-Natal Belt: evidence from deep borehole intersections in South Africa, Precambrian Research 125, 179–189.

Evans, R. K., 1965, The Geology of the Shire Highlands, Bulletin 18, Geological Survey of Malawi, Government Printer, Zomba, Malawi.

Fisher C. M., Hanchar J. M., Samson S. D., Dhuime B., Blichert-Toft J., Vervoort J. D., Lam R., Synthetic zircon doped with hafnium and rare earth elements: A reference material for in situ hafnium isotope analysis, 2011, Chemical Geology, Volume 286, Issues 1–2, 26 June 2011, Pages 32–47.

Furman, T., Graham, D., 1999, Erosion of lithospheric mantle beneath the East African Rift system: geochemical evidence from the Kivu volcanic province. Lithosphere 48, 237–262.

Garson, M. S. and Walshaw R.D., 1969, The Geology of the Mulanje Area, Bulletin 21, Geological Survey of Malawi, Government Printer, Zomba, Malawi.

Grantham G. H., Maboko M. & Eglington B. M., 2003, A review of the evolution of the Mozambique Belt and implications for the amalgamation and dispersal of Rodinia and Gondwana, Geological Society, London, Special Publications, 206, 401-425. 0305-8719/03/$15.

Griffin W.L., E.A. Belousova, S.R. Shee, N.J. Pearson, S.Y. O'Reilly, 2004, Archean crustal evolution in the northern Yilgarn Craton: U–Pb and Hf-isotope evidence from detrital zircons, Precambrian Research 131 (2004) 231–282

Hanson R. E., 2003, Proterozoic geochronology and tectonic evolution of southern Africa, Geological Society, London, Special Publications, volume 206, pages 427 – 463, doi: 10.1144/GSL.SP.2003.206.01.20

Hauzenberger, Christoph & Tenczer, V & Bauernhofer, A & Fritz, Harald & Urs, Kloetzli & Košler, J & Wallbrecher, Eckart & Muhongo, S. 2014. Termination of the Southern Irumide Belt in Tanzania: Zircon U/Pb geochronology. Precambrian Research. 255. 10.1016/j.precamres.2014.09.021.

Hiess J., Condon D. J., McLean N. and Noble S. R., 2012, 238U/235U systematics in terrestrial U-bearing minerals, Science Magazine, New York, N.Y.), volume 335, no. 6076, pages 1610-4, doi: 1126/science.1215507.

Jackson S. E., Pearson N. J., Griffin W. L., Belousova E. A., 2004, The application of laser ablation-inductively coupled plasma-mass spectrometry to in situ U–Pb zircon geochronology, Chemical Geology, Volume 211, Issues 1–2, Pages 1-184 (8 November 2004) Original Research Article, Pages 47-69.

Jacobs J., C. Mark Fanning, Friedhelm Henjes-Kunst, Martin Olesch, and Hans-Ju¨ rgen Paech, Continuation of the Mozambique Belt into East Antarctica: Grenville-Age Metamorphism and Polyphase Pan-African High-Grade Events in Central Dronning Maud Land, 1998, The Journal of Geology, Vol. 106, No. 4 (July 1998), pp. 385-406, The University of Chicago Press, Stable URL: http://www.jstor.org/stable/10.1086/516031, Accessed: 10/12/2015 18:21

Jacobs, J. and R. J. Thomas, 2004, "Himalayan-type indenter-escape tectonics model for the southern part of the late Neoproterozoic-early Palaeozoic East African-Antarctic orogen." Geology 32(8): 721-724.

Jacobs, J., Pisarevsky, S., Thomas, R.J., Becker, T., 2008. The Kalahari Craton during the assembly and dispersal of Rodinia. Precambrian Research 160, 142–158

.

Johnson S.P., Cutten H.N.C., Muhongo S., De Waele B., 2003, Neoarchaean Magmatism and Metamorphism of the Western Granulites in the Central Domain of the Mozambique Belt,

TANZANIA: U–PB SHRIMP GEOCHRONOLOGY AND PT ESTIMATES, TECTONOPHYSICS 375 (2003) 125–145

JOHNSON S. P, T. RIVERS & B. DE WAELE, 2005, A REVIEW OF THE MESOPROTEROZOIC TO EARLY PALAEOZOIC MAGMATIC AND TECTONOTHERMAL HISTORY OF SOUTH–CENTRAL AFRICA: IMPLICATIONS FOR RODINIA AND GONDWANA, JOURNAL OF THE GEOLOGICAL SOCIETY, LONDON, VOL. 162, 2005, PP. 433–450. PRINTED IN GREAT BRITAIN.

JOHNSON S. P., B. DE WAELE, AND K. A. LIYUNGU, 2006, U-PB SENSITIVE HIGH-RESOLUTION ION MICROPROBE (SHRIMP) ZIRCON GEOCHRONOLOGY OF GRANITOID ROCKS IN EASTERN ZAMBIA: TERRANE SUBDIVISION OF THE MESOPROTEROZOIC SOUTHERN IRUMIDE BELT, TECTONICS, VOLUME 25, TC6004, DOI:10.1029/2006TC001977, 2006.

JOHNSON S. P., B. DE WAELE, F. TEMBO, C. KATONGO, K. TANI, Q.CHANG, T. IIZUKA, D. DUNKLEY, 2007, GEOCHEMISTRY, GEOCHRONOLOGY AND ISOTOPIC EVOLUTION OF THE CHEWORE-RUFUNSA TERRANE, SOUTHERN IRUMIDE BELT: A MESOPROTEROZOIC CONTINENTAL MARGIN ARC, JOURNAL OF PETROLOGY, VOLUME 48, NUMBER 7, PAGES 1411-1441, 2007, DOI:10.1093/PETROLOGY/EGM025

KRÖNER A., WILLNER A. P., HEGNER E., JAECKEL P., NEMCHIN A., 2001. "SINGLE ZIRCON AGES, PT EVOLUTION AND ND ISOTOPIC SYSTEMATICS OF HIGH-GRADE GNEISSES IN SOUTHERN MALAWI AND THEIR BEARING ON THE EVOLUTION OF THE MOZAMBIQUE BELT IN SOUTH-EASTERN AFRICA." PRECAMBRIAN RESEARCH 109(3-4): 257-291.

KRÖNER A., & U. CORDANI, 2003, AFRICAN, SOUTHERN INDIAN AND SOUTH AMERICAN CRATONS WERE NOT PART OF THE RODINIA SUPERCONTINENT: EVIDENCE FROM FIELD RELATIONSHIPS AND GEOCHRONOLOGY, TECTONOPHYSICS 375 (2003) 325– 352.

Li, Z. X., S. V. Bogdanova, et al. 2008, "Assembly, configuration, and break-up history of Rodinia: A synthesis." Precambrian Research 160(1–2): 179-210.

Ludwig, K.R., 2003, Isoplot 3.00: A geochronological toolkit for Microsoft Excel: Berkeley Geochronology Centre Special Publication 4, 70 p.

Macey P.H., R.J. Thomas, G.H. Grantham, B.A. Ingram, J. Jacobs, R.A. Armstrong, M.P. Roberts, B. Bingen, L. Hollick, G.S. de Kock, G. Viola,W. Bauer, E. Gonzales, T. Bjerkgård, I.H.C. Henderson, J.S. Sandstad, M.S. Cronwright, S. Harley, A. Solli, Ø. Nordgulen, G. Motuza, E. Daudi, V. Manhica¸ 2010, Mesoproterozoic geology of the Nampula Block, northern Mozambique: Tracing fragments of Mesoproterozoic crust in the heart of Gondwana, Precambrian Research 182 (2010) 124–148

Meert, J. G. and R. Van Der Voo 1997, "The assembly of Gondwana 800-550 Ma." Journal of Geodynamics 23(3–4): 223-235.

Meert, J. G. 2003, "A synopsis of events related to the assembly of eastern Gondwana." Tectonophysics 362(1–4): 1-40.

Muhongo S. & Lenoir J. L., 1994, Pan-African Granulite-Facies Metamorphism in the Mozambique Belt of Tanzania: U-Pb Zircon Geochronology, Journal of the Geological Society, London, Vol. 151, 1994, Pp. 343-347.

Muhongo S., Hauzenberger C., and Sommer H., 2003, Vestiges of the Mesoproterozoic Events in the Neoproterozoic Mozambique Belt: The East African Perspective in the Rodinia Puzzle, Gondwana Research, V 6, No. 3, pp. 409-41 6.

Norry, M.J., Truckle, P.H., Lippard, S.J., Hawkesworth, C.J., Weaver, S.D., Marriner, G.F., Bailey, D.K., 1980, Isotopic and trace element evidence from lavas, bearing on mantle heterogeneity beneath Kenya. Philosophical Transactions. Series A, Mathematical, Physical, and Engineering Sciences, Royal Society of London, 297, 259–271.

Nowell, G and Parrish, R.R., 2001, Simultaneous Acquisition of Isotope Compositions and Parent/Daughter Ratios by non-isotope-dilution-mode Plasma Ionisation Multi-collector Mass Spectrometer (PIMMS), in Plasma Source Mass Spectrometer: The New Millennium, edited by G. Holland and S.D. Tanner, Proceedings of the 7th International Conference of Plasma Source Mass Spectrometry: The Millennium Conference, Royal Society of Chemistry, Special Publication 267, pp 298 - 310

Pinna, P., G. Jourde, et al. 1993. "The Mozambique Belt in northern Mozambique: Neoproterozoic (1100–850 Ma) crustal growth and tectogenesis, and superimposed Pan-African (800–550 Ma) tectonism." Precambrian Research 62(1–2): 1-59.

Ray J., Saha A., Ganguly S., Balaram V, Krishna A K., and Hazra S., 2011, Geochemistry and Petrogenesis of Neoproterozoic Mylliem Granitoids, Meghalaya Plateau, Northeastern India, Journal of Earth System Science, 120, No. 3, June 2011, pp. 459–473, Indian Academy of Sciences.

Sacchi, R., J. Marques, et al., 1984, Kibaran events in the southernmost Mozambique belt. Precambrian Research, 25, 141–159.

Sláma J., Košler J., Condon D. J., Crowley J. L., Gerdes A., Hanchar J. M., Horstwood M. S.A., Morris G. A., Nasdala L., Norberg N., Schaltegger U., Schoene B., Tubrett M. N., Sommer H., A. Kröner, C. Hauzenberger, S. Muhongo and M. T. D. Wingate, 2003, Metamorphic petrology and zircon geochronology of high-grade rocks from the central Mozambique Belt of Tanzania: crustal recycling of Archean and Paleoproterozoic material during the Pan-African orogeny, Journal of metamorphic Geology, 2003, 21, 915–934 doi:10.1046/j.1525-1314.2003. 00491.x

SPENCER, C.J., HAWKESWORTH, C., CAWOOD, P. A., DHUIME, B., 2013, NOT ALL SUPERCONTINENTS ARE CREATED EQUAL: GONDWANA-RODINIA CASE STUDY. GEOLOGY 41, 795–798. DOI:10.1130/G34520.1

SPENCER, C.J., ROBERTS, N.M.W., CAWOOD, P.A., HAWKESWORTH, C.J., PRAVE, A.R., ANTONINI, A.S.M., HORSTWOOD, M.S.A., 2014, INTERMONTANE BASINS AND BIMODAL VOLCANISM AT THE ONSET OF THE SVECONORWEGIAN OROGENY, SOUTHERN NORWAY. PRECAMBRIAN RESEARCH, 252, 107–118.

SPENCER, C.J., KIRKLAND, C.L., TAYLOR, R.J.M., 2016, STRATEGIES TOWARDS STATISTICALLY ROBUST INTERPRETATIONS OF IN SITU U-PB ZIRCON GEOCHRONOLOGY. GEOSCIENCE FRONTIERS. 7, 581–589. DOI:10.1016/J.GSF.2015.11.006

SPENCER, C.J., YAKYMCHUK, C., GHAZNAVI, M., 2017, VISUALISING DATA DISTRIBUTIONS WITH KERNEL DENSITY ESTIMATION AND REDUCED CHI-SQUARED STATISTIC. GEOSCIENCE FRONTIERS 8, 1247–1252. DOI:10.1016/J.GSF.2017.05.002

STERN R. J., 1994, ARC ASSEMBLY AND CONTINENTAL COLLISION IN THE NEOPROTEROZOIC EAST AFRICAN OROGEN: IMPLICATIONS FOR THE CONSOLIDATION OF GONDWANALAND, ANNUAL REVIEWS OF EARTH AND PLANETARY SCIENCES, 1994. 22: 319-51.

STERN, R. J. 2002, "CRUSTAL EVOLUTION IN THE EAST AFRICAN OROGEN: A NEODYMIUM ISOTOPIC PERSPECTIVE." JOURNAL OF AFRICAN EARTH SCIENCES 34(3–4): 109-117.

STERN R. J., 2002, CRUSTAL EVOLUTION IN THE EAST AFRICAN OROGEN: A NEODYMIUM ISOTOPIC PERSPECTIVE, JOURNAL OF AFRICAN EARTH SCIENCES, 34 (2002) 109–117.

TANAKA T., TOGASHI S., KAMIOKA H., AMAKAWA H., KAGAMI H., HAMAMOTO T., YUHARA M., ORIHASHI Y., YONEDA S., SHIMIZU H., KUNIMARU T., TAKAHASHI K., 2000, JNDI-1: A NEODYMIUM ISOTOPIC REFERENCE IN CONSISTENCY WITH LAJOLLA NEODYMIUM, CHEMICAL GEOLOGY - CHEM GEOL, VOL. 168, NO. 3, PP. 279-281, 2000, DOI: 10.1016/S0009-2541(00)00198-4

Thomas, R.J., Spencer, C., Bushi, A.M., Baglow, N., Boniface, N., de Kock, G., Horstwood, M.S.A., Hollick, L., Jacobs, J., Kajara, S., Kamihanda, G., Key, R.M., Maganga, Z., Mbawala, F., McCourt, W., Momburi, P., Moses, F., Mruma, A., Myambilwa, Y., Roberts, N.M.W., Saidi, H., Nyanda, P., Nyoka, K., Millar, I., 2016a. Geochronology of the central Tanzania Craton and its southern and eastern orogenic margins. Precambrian Research, 277. doi:10.1016/j.precamres.2016.02.008

Thomas, R.J., Macey, P.H., Spencer, C., Dhansay, T., Diener, J.F.A., Lambert, C.W., Frei, D., Nguno, A., 2016b, The Sperrgebiet Domain, Aurus Mountains, SW Namibia: A 2020–850 Ma window within the Pan-African Gariep Orogen. Precambrian Research, 286. doi:10.1016/j.precamres.2016.09.023

Westerhof, A. B. Phil, Lehtonen, M. I., Mäkitie, H., Manninen, T., Pekkala, Y., Gustafsson, B. & Tahon, A. 2007, The Tete-Chipata Belt: A New Multiple Terrane Element from Western Mozambique and Southern Zambia, GTK Consortium Geological Surveys in Mozambique 2002–2007, edited by Yrjö Pekkala, Tapio Lehto & Hannu Mäkitie.

Wiedenbeck M., Hanchar J. M., Peck W. H., Sylvester P., Valley J., Whitehouse M., Kronz A., Morishita Y., Nasdala L., Fiebig J., Franchi I., Girard J.-P., Greenwood R.C., Hinton R., Kita N., Mason P.R.D., Norman M., Ogasawara M., Piccoli P.M., Rhede D., Satoh H., Schulz-Dobrick B., Skår O., Spicuzza M.J., Terada K., Tindle A., Togashi S., Vennemann T., Xie Q., and Zheng Y.-F., 2004, Further Characterisation of the 91500 Zircon Crystal, Geostandards and Geoanalytical Research, Volume 28, Issue 1, pages 9–39, DOI: 10.1111/j.1751-908X.2004.tb01041.x.

Woolley A. R. & Jones G. C. 1987, The Petrochemistry of the northern part of the Chilwa Alkaline Province, Malawi, Geological Society Special Publication No. 30, pp. 335-355.

XU Y, CAWOOD P. A., DU Y., HUGHES N. C., 2014, TERMINAL SUTURING OF GONDWANA ALONG THE SOUTHERN MARGIN OF SOUTH CHINA CRATON: EVIDENCE FROM DETRITAL ZIRCON U-PB AGES AND HF ISOTOPES IN CAMBRIAN AND ORDOVICIAN STRATA, HAINAN ISLAND, TECTONICS, VOLUME 33, ISSUE 12, DECEMBER 2014, PAGES 2490–2504

Table 1: Analysed sample numbers, GPS locations, rock type and zircon age. Abbreviations: M – metamorphic age.:

Sample No	Locality GPS	Rock type	Age (Ma)	2S	MSWD	U-Pb age type	εHf	2S	Model age (TDM)
BM 163	-15.6912700 +34.4177300	Metagranite	1038	12	1.18	Upper intercept	+6.1	0.6	1877
BM 174	-15.7080300 +34.5266700	Metagranite	1036	8	1.2	Upper intercept	+4.8	0.7	1942
BM 179	-15.5522500 +34.4933800	Metagranite	1047	12	1.01	Upper intercept	+4.7	0.7	1952
BM 200	-15.3636700 +34.5678000	Qtz-felds gneiss	1031 607	34 41	4.0 5.0	Weighted average Weighted average	+9.2 -0.1	1.0 1.1	1616 1586
BM 209	-15.7139300 +34.7369600	Metagranite	1040	5	2.1	Upper intercept	+6.8	2.1	1833
BM213G	-15.7769000 +34.4452700	Metagranite	1088	23	1.5	Upper intercept	+6.9	2.3	1898
BM 213X	-15.7769000 +34.4452700	Xenolith	1034	15	1.08	Upper intercept	+5.7	2.6	1888
BM 221	-15.0201600 +35.1322900	Leucogranite gneiss	735	69	0.24	Weighted average	+4.5	0.45	1592
BM	-	Hornblen	956	1	0.9	Weighted	+	1	1762

223A	15.0246800 +35.1206 600	de biotite gneiss		2	3	average	6.9	.3	
BM 240	- 16.0511100 +35.7783 500	Granite	118	1 .2	1.5	Lower intercept	- 5.4	1 .0	1383
BM 249	- 15.8338600 +35.5992 400	Charnockitic gneiss	1036	15	2.0	Upper intercept	+ 6.4	0 .8	1836
BM 252	- 16.1406400 +35.0914 900	Charnockitic gneiss	1128 515	30 18	1.1 1.1	Upper intercept Lower intercept (M)	N /A	N /A	N/A
BM 256	- 16.3755300 +35.1994 800	Metagranite	1070	16	0.97	Upper intercept	+ 6.1	1 .3	1937
BM 281	- 15.4565600 +35.2863 100	Charnockitic gneiss	594 493	65 22	1.4 0.12	Upper intercept M	+ 6.8	1 .2	1865
BM282A	- 15.4925100 +35.2291 100	Charnockitic gneiss	1187 536	53 24	3.7 3.7	Upper intercept Lower intercept	+ 9.2 + 2.3	1 .3 1 .3	1335 1472
BM 282 B	- 15.4925100 +35.2291	Charnockitic gneiss	715 580	18	3.5 3.5	Upper intercept	N /A	N /A	N/A

	100			9 9		Lower intercept			
BM 289	- 15.6907200 +35.1889 900	Perthitic syenite	531	3 .4	0.4 7	Weighted average	+ 1.6	1 .3	1675

Table 2: Summary of Lu-Hf spot analyses for foliated granites and charnockitic gneisses

Sample	Rock type	U - Pb Age	Initial εHf(t)	Mean εHf(t)	Model ages (TDM) range (Ma)	Mean model age (Ma)
BM 163	Foliated granite	1038	+5.2 to +6.8	+6.1	1920 to 1833	1877
BM 174	Foliated granite	1036	+3.9 to +5.7	+4.8	1984 to 1890	1942
BM 179	Foliated granite	1036	+3.8 to +5.4	+4.7	1992 to 1912	1952
BM 209	Foliated granite	1033	+5.8 to +7.8	+6.8	1890 to 1774	1833
BM 213G	Foliated granite	1088	+6.0 to +8.4	+6.9	1947 to 1814	1898
BM 213X	Foliated granite	1034	+4.5 to +7.0	+5.7	1961 to 1822	1888
BM 256	Foliated granite	1070	+5.1 to +6.5	+6.1	1977 to 1891	1937
BM 249	Charnockitic gneiss	1036	+5.5 to +7.8	+6.4	1901 to 1832	1836
BM 282A	Charnockitic gneiss	1100	+8.9 to +9.2	+9.2	1791 to 1730	1335
BM 200	Quartzfelspathic gneiss	1031	+7.7 to +10.3	+9	1761 to 1443	1602
BM 221	Leucogranite	756	+4.3 to +4.6	+ 4.5	1599 to 1585	1592
BM 223A	Hornblende biotite gneiss	956	+5.5 to +8.1	+ 6. 8	1813 to 1670	1744
BM 289	Perthitic syenite	531	-2.7 to + 1.4	- 1	1496 to 1742	1619
BM 240	Granite	124	-7.2 to -3.8	- 5.5	1479 to 1293	1386

HIGHLIGHTS

- Periods of magmatic activity: Mesoproterozoic, Neoproterozoic, Cambrian, Mesozoic.
- Oldest magmatism 1128 ± 30 Ma (charnockitic gneiss). Metamorphism (515 ± 18 Ma).
- Radiogenic isotope data: Mesoproterozoic rocks with positive εNd and εHf values.

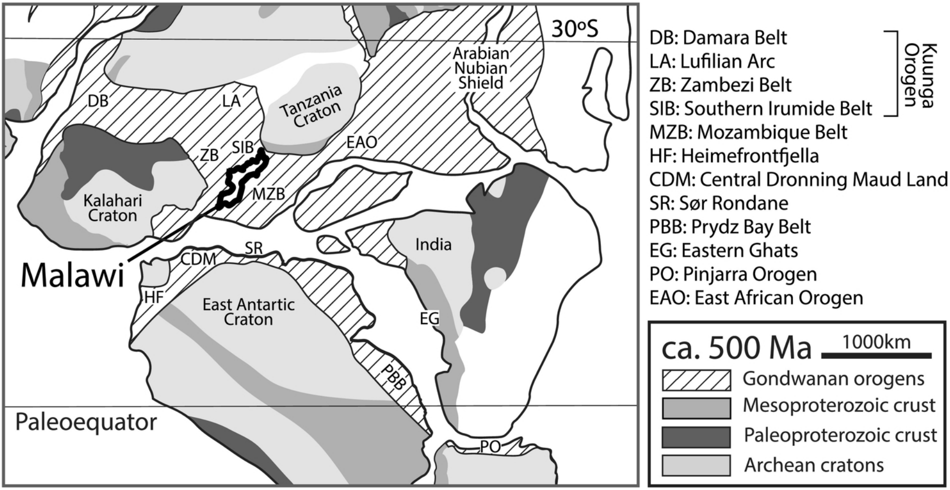

30°S
Arabian Nubian Shield
DB
LA
Tanzania Craton
ZB
SIB
EAO
MZB
Kalahari Craton
Malawi
SR
CDM
HF
East Antartic Craton
India
EG
PBB
PO
Paleoequator
DB: Damara Belt
LA: Lufilian Arc
ZB: Zambezi Belt
SIB: Southern Irumide Belt
Kuunga Orogen
MZB: Mozambique Belt
HF: Heimefrontfjella
CDM: Central Dronning Maud Land
SR: Sør Rondane
PBB: Prydz Bay Belt
EG: Eastern Ghats
PO: Pinjarra Orogen
EAO: East African Orogen
ca. 500 Ma
1000km
Gondwanan orogens
Mesoproterozoic crust
Paleoproterozoic crust
Archean cratons

Figure 1

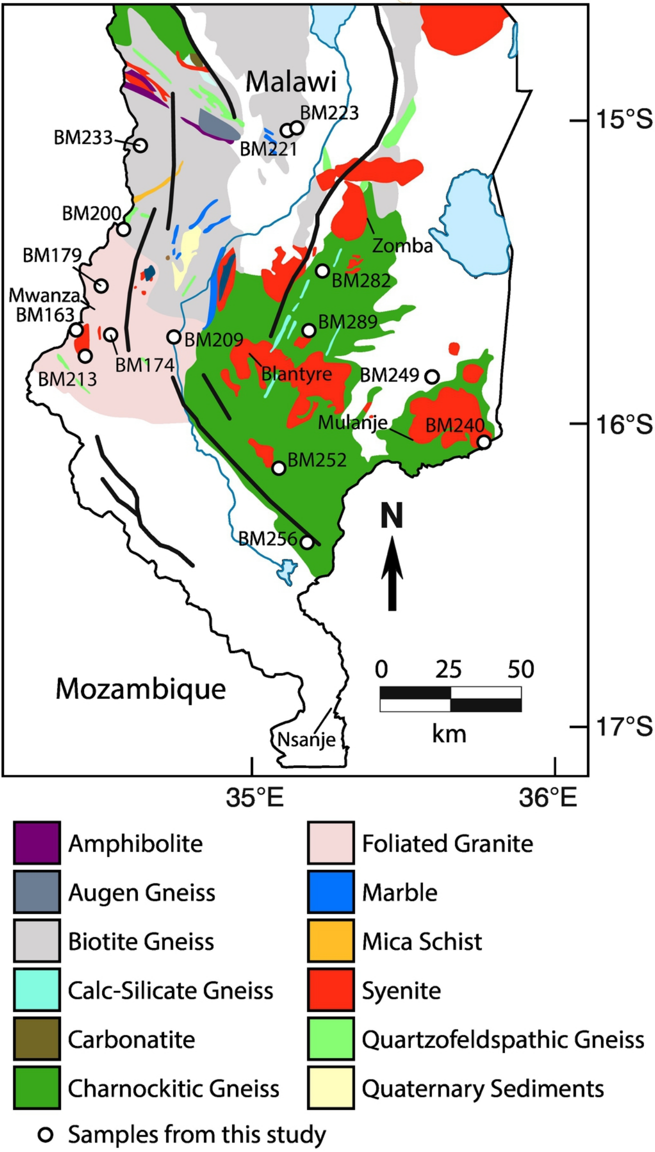

Malawi
Mozambique
BM223
BM221
BM233
BM200
BM179
Mwanza
BM163
BM174
BM209
BM213
BM282
BM289
BM249
BM240
BM252
BM256
Zomba
Blantyre
Mulanje
Nsanje
15°S
16°S
17°S
35°E
36°E
N
0
25
50
km
Amphibolite
Augen Gneiss
Biotite Gneiss
Calc-Silicate Gneiss
Carbonatite
Charnockitic Gneiss
Foliated Granite
Marble
Mica Schist
Syenite
Quartzofeldspathic Gneiss
Quaternary Sediments
Samples from this study

Figure 2

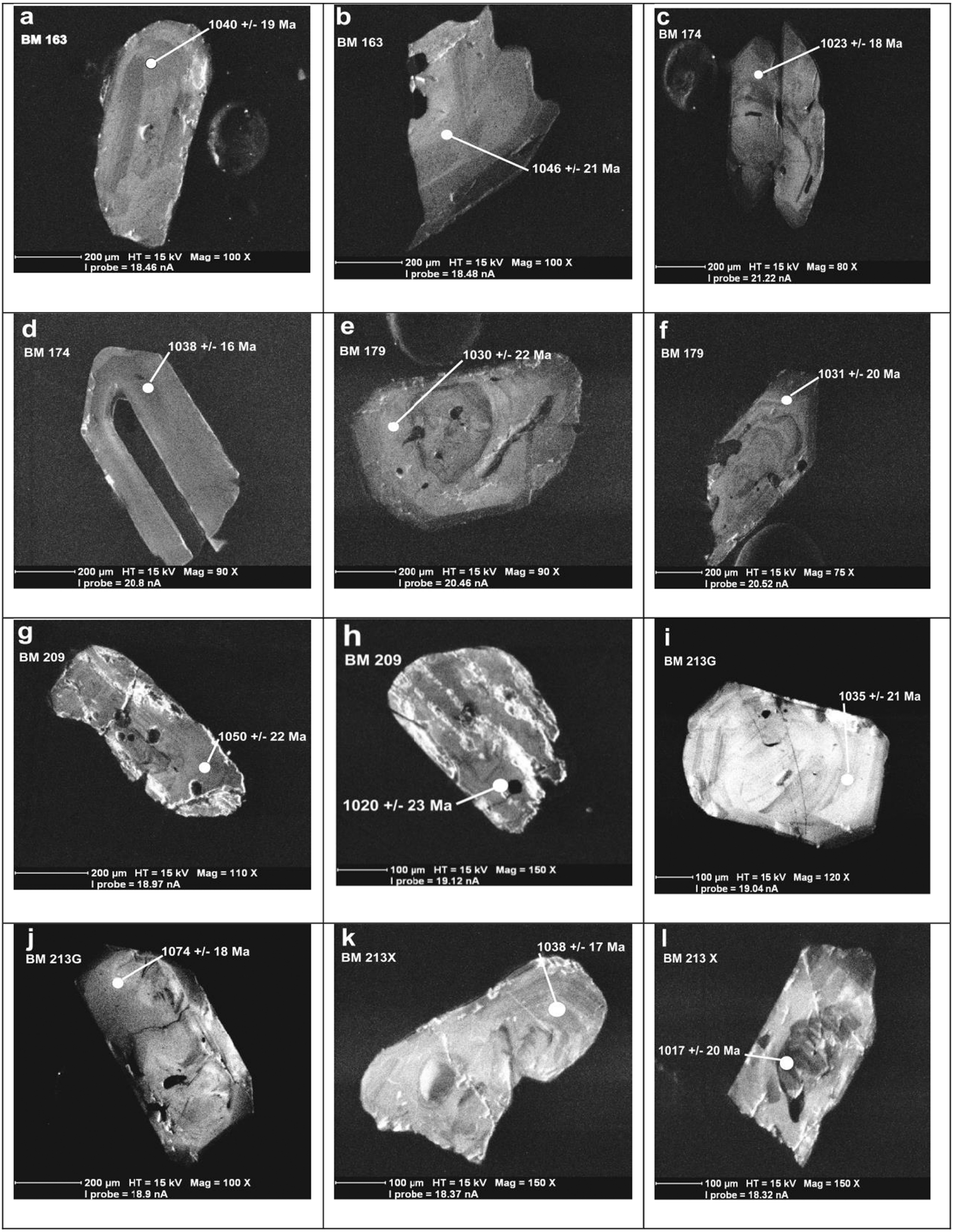
a
BM 163
1040 +/- 19 Ma
200 µm HT = 15 kV Mag = 100 X
I probe = 18.46 nA
b
BM 163
1046 +/- 21 Ma
200 µm HT = 15 kV Mag = 100 X
I probe = 18.48 nA
c
BM 174
1023 +/- 18 Ma
200 µm HT = 15 kV Mag = 80 X
I probe = 21.22 nA
d
BM 174
1038 +/- 16 Ma
200 µm HT = 15 kV Mag = 90 X
I probe = 20.8 nA
e
BM 179
1030 +/- 22 Ma
200 µm HT = 15 kV Mag = 90 X
I probe = 20.46 nA
f
BM 179
1031 +/- 20 Ma
200 µm HT = 15 kV Mag = 75 X
I probe = 20.52 nA
g
BM 209
1050 +/- 22 Ma
200 µm HT = 15 kV Mag = 110 X
I probe = 18.97 nA
h
BM 209
1020 +/- 23 Ma
100 µm HT = 15 kV Mag = 150 X
I probe = 19.12 nA
i
BM 213G
1035 +/- 21 Ma
100 µm HT = 15 kV Mag = 120 X
I probe = 19.04 nA
j
BM 213G
1074 +/- 18 Ma
200 µm HT = 15 kV Mag = 100 X
I probe = 18.9 nA
k
BM 213X
1038 +/- 17 Ma
100 µm HT = 15 kV Mag = 150 X
I probe = 18.37 nA
l
BM 213 X
1017 +/- 20 Ma
100 µm HT = 15 kV Mag = 150 X
I probe = 18.32 nA

Figure 3al

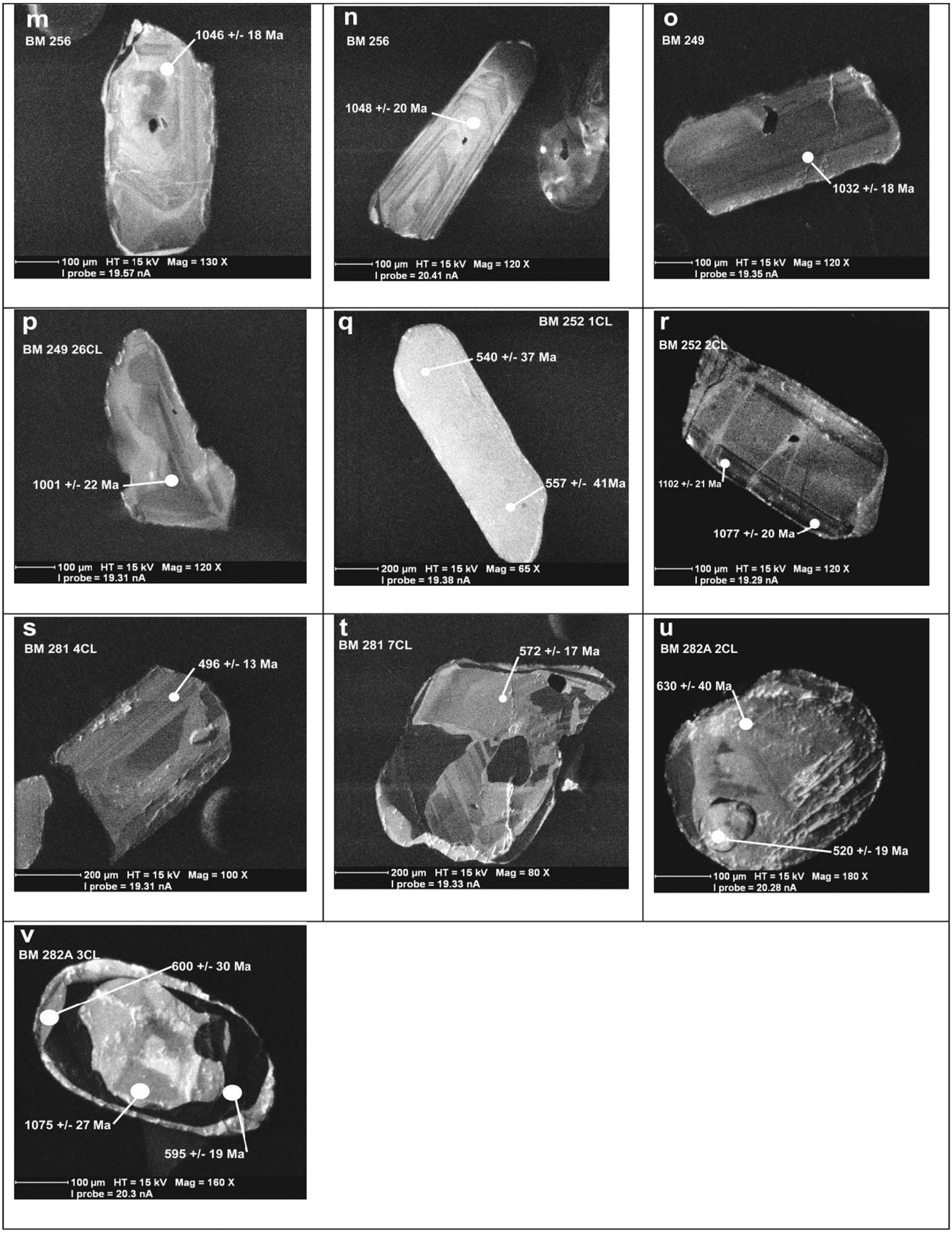
m
BM 256
1046 +/- 18 Ma
100 µm HT = 15 kV Mag = 130 X
I probe = 19.57 nA
n
BM 256
1048 +/- 20 Ma
100 µm HT = 15 kV Mag = 120 X
I probe = 20.41 nA
o
BM 249
1032 +/- 18 Ma
100 µm HT = 15 kV Mag = 120 X
I probe = 19.35 nA
p
BM 249 26CL
1001 +/- 22 Ma
100 µm HT = 15 kV Mag = 120 X
I probe = 19.31 nA
q
BM 252 1CL
540 +/- 37 Ma
557 +/- 41Ma
200 µm HT = 15 kV Mag = 65 X
I probe = 19.38 nA
r
BM 252 2CL
1102 +/- 21 Ma
1077 +/- 20 Ma
100 µm HT = 15 kV Mag = 120 X
I probe = 19.29 nA
s
BM 281 4CL
496 +/- 13 Ma
200 µm HT = 15 kV Mag = 100 X
I probe = 19.31 nA
t
BM 281 7CL
572 +/- 17 Ma
200 µm HT = 15 kV Mag = 80 X
I probe = 19.33 nA
u
BM 282A 2CL
630 +/- 40 Ma
520 +/- 19 Ma
100 µm HT = 15 kV Mag = 180 X
I probe = 20.28 nA
v
BM 282A 3CL
600 +/- 30 Ma
1075 +/- 27 Ma
595 +/- 19 Ma
100 µm HT = 15 kV Mag = 160 X
I probe = 20.3 nA

Figure 3mv

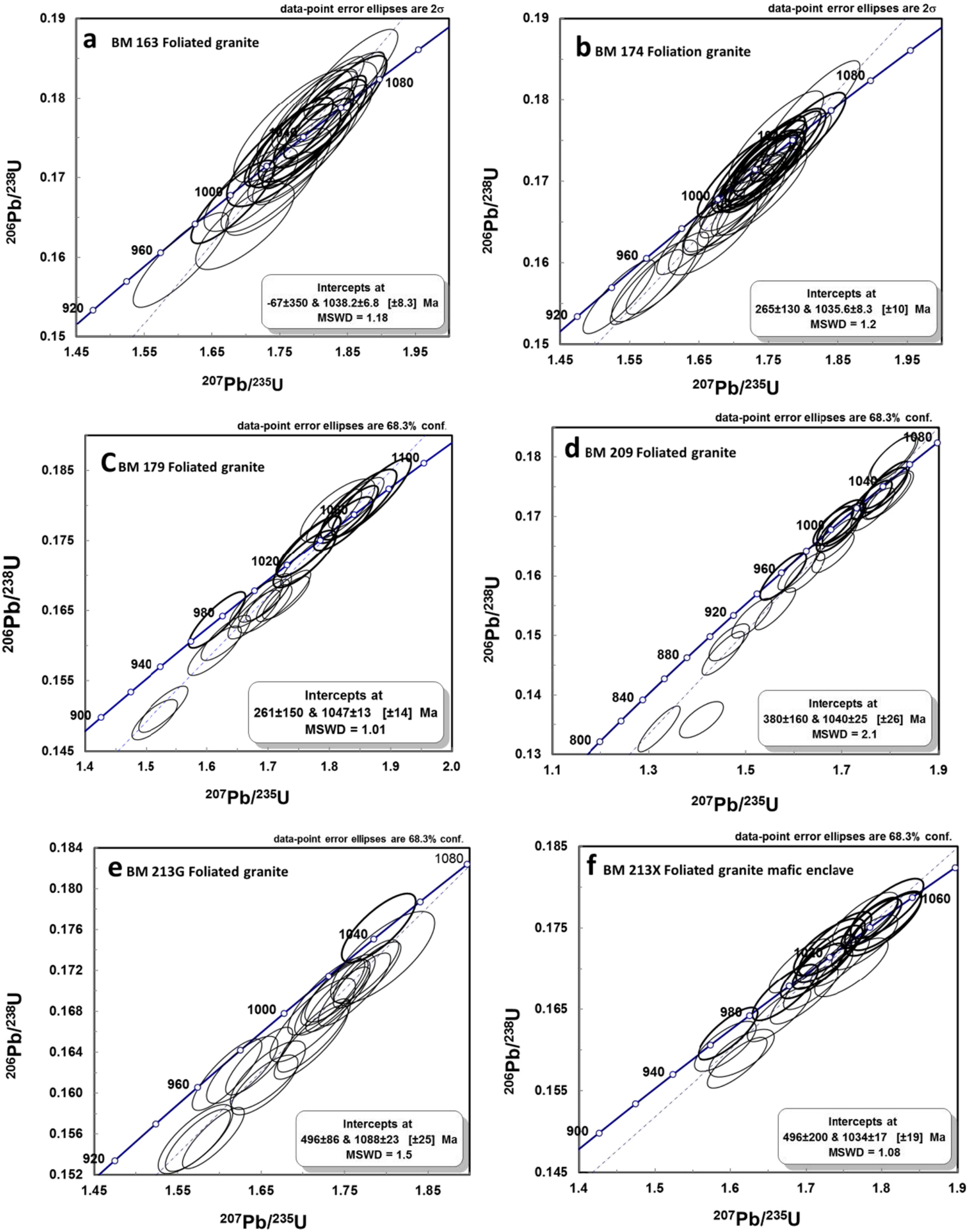

data-point error ellipses are 2σ
a BM 163 Foliated granite
Intercepts at
-67±350 & 1038.2±6.8 [±8.3] Ma
MSWD = 1.18
b BM 174 Foliation granite
Intercepts at
265±130 & 1035.6±8.3 [±10] Ma
MSWD = 1.2
data-point error ellipses are 68.3% conf.
C BM 179 Foliated granite
Intercepts at
261±150 & 1047±13 [±14] Ma
MSWD = 1.01
d BM 209 Foliated granite
Intercepts at
380±160 & 1040±25 [±26] Ma
MSWD = 2.1
e BM 213G Foliated granite
Intercepts at
496±86 & 1088±23 [±25] Ma
MSWD = 1.5
f BM 213X Foliated granite mafic enclave
Intercepts at
496±200 & 1034±17 [±19] Ma
MSWD = 1.08
206Pb/238U
207Pb/235U

Figure 4af

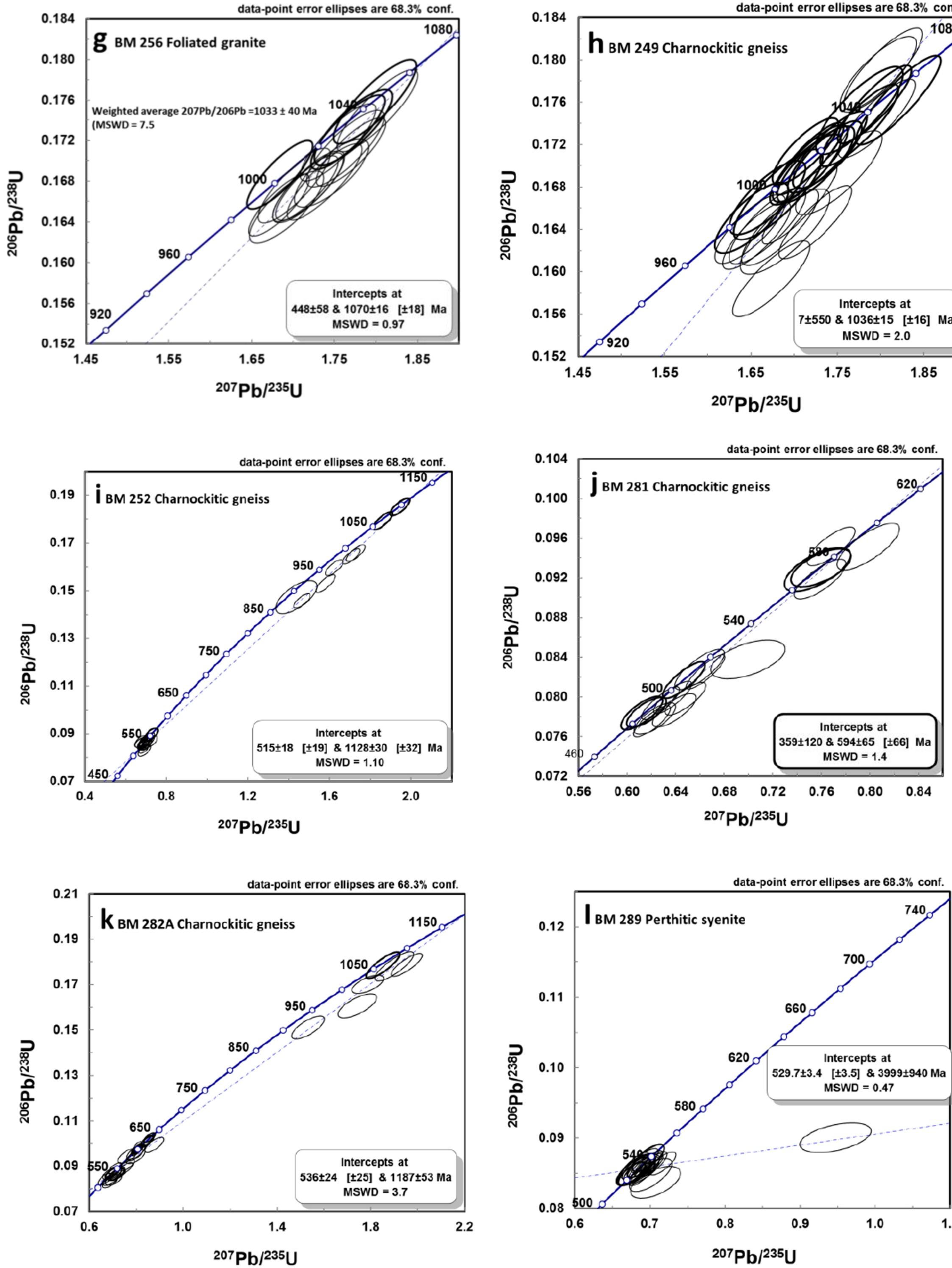

data-point error ellipses are 68.3% conf.
g BM 256 Foliated granite
Weighted average 207Pb/206Pb =1033 ± 40 Ma
(MSWD = 7.5
Intercepts at
448±58 & 1070±16 [±18] Ma
MSWD = 0.97
h BM 249 Charnockitic gneiss
Intercepts at
7±550 & 1036±15 [±16] Ma
MSWD = 2.0
i BM 252 Charnockitic gneiss
Intercepts at
515±18 [±19] & 1128±30 [±32] Ma
MSWD = 1.10
j BM 281 Charnockitic gneiss
Intercepts at
359±120 & 594±65 [±66] Ma
MSWD = 1.4
k BM 282A Charnockitic gneiss
Intercepts at
536±24 [±25] & 1187±53 Ma
MSWD = 3.7
l BM 289 Perthitic syenite
Intercepts at
529.7±3.4 [±3.5] & 3999±940 Ma
MSWD = 0.47
206Pb/238U
207Pb/235U

Figure 4gl

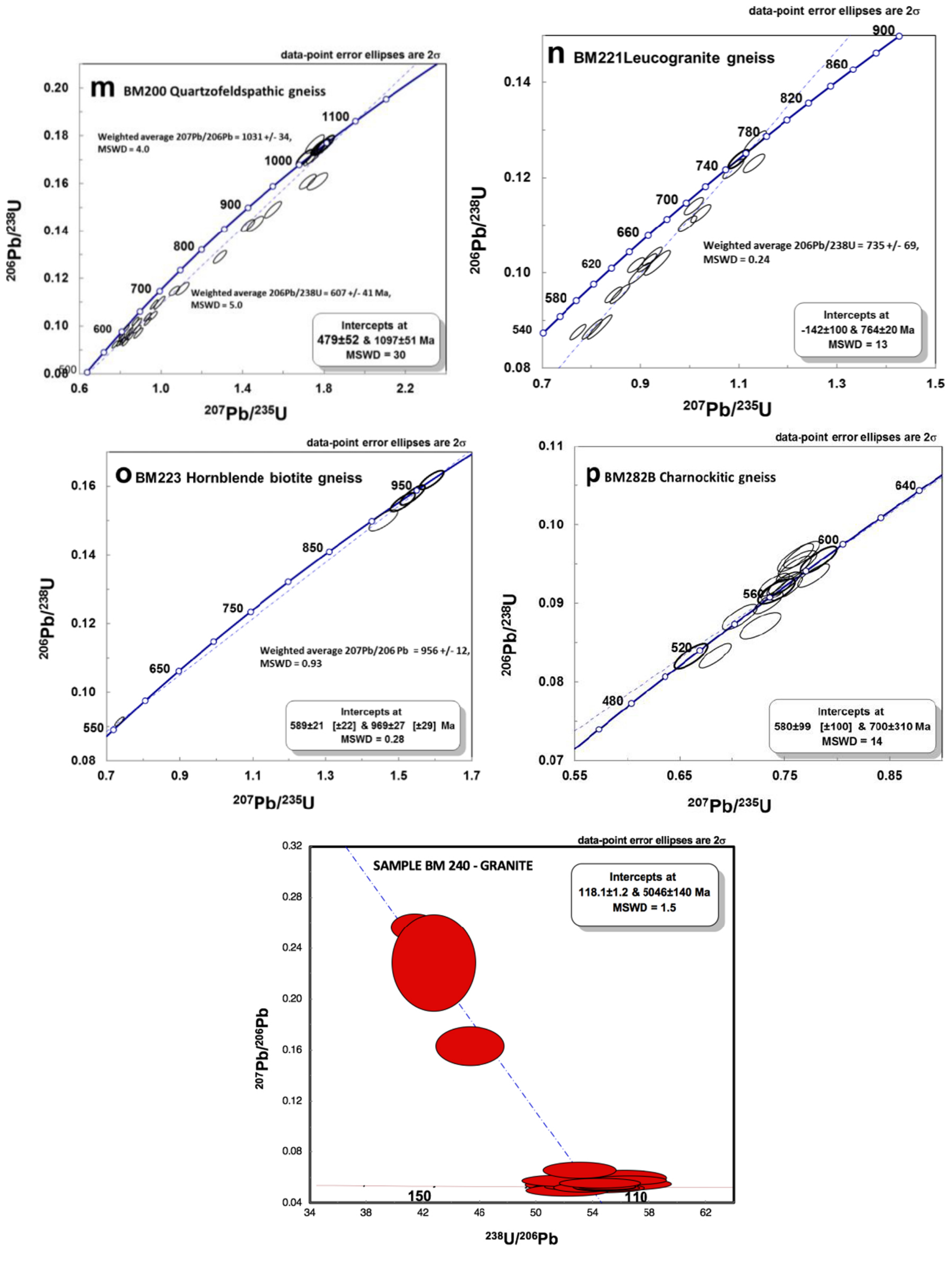
data-point error ellipses are 2σ
m BM200 Quartzofeldspathic gneiss
Weighted average 207Pb/206Pb = 1031 +/- 34, MSWD = 4.0
Weighted average 206Pb/238U = 607 +/- 41 Ma, MSWD = 5.0
Intercepts at 479±52 & 1097±51 Ma MSWD = 30
206Pb/238U
207Pb/235U
data-point error ellipses are 2σ
n BM221Leucogranite gneiss
Weighted average 206Pb/238U = 735 +/- 69, MSWD = 0.24
Intercepts at -142±100 & 764±20 Ma MSWD = 13
206Pb/238U
207Pb/235U
data-point error ellipses are 2σ
o BM223 Hornblende biotite gneiss
Weighted average 207Pb/206 Pb = 956 +/- 12, MSWD = 0.93
Intercepts at 589±21 [±22] & 969±27 [±29] Ma MSWD = 0.28
206Pb/238U
207Pb/235U
data-point error ellipses are 2σ
p BM282B Charnockitic gneiss
Intercepts at 580±99 [±100] & 700±310 Ma MSWD = 14
206Pb/238U
207Pb/235U
data-point error ellipses are 2σ
SAMPLE BM 240 - GRANITE
Intercepts at 118.1±1.2 & 5046±140 Ma MSWD = 1.5
207Pb/206Pb
238U/206Pb

Figure 4mp

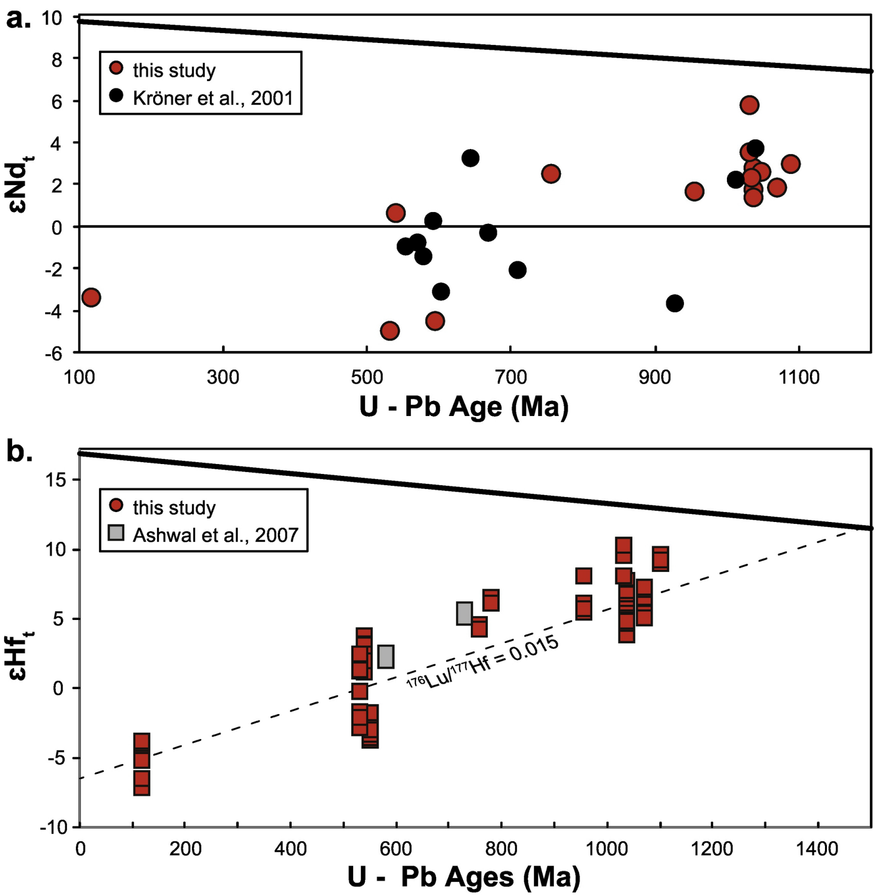

a.
this study
Kröner et al., 2001
εNd$_t$
U - Pb Age (Ma)
10
8
6
4
2
0
-2
-4
-6
100
300
500
700
900
1100
b.
this study
Ashwal et al., 2007
εHf$_t$
^{176}Lu/^{177}Hf = 0.015
U - Pb Ages (Ma)
15
10
5
0
-5
-10
0
200
400
600
800
1000
1200
1400

Figure 5

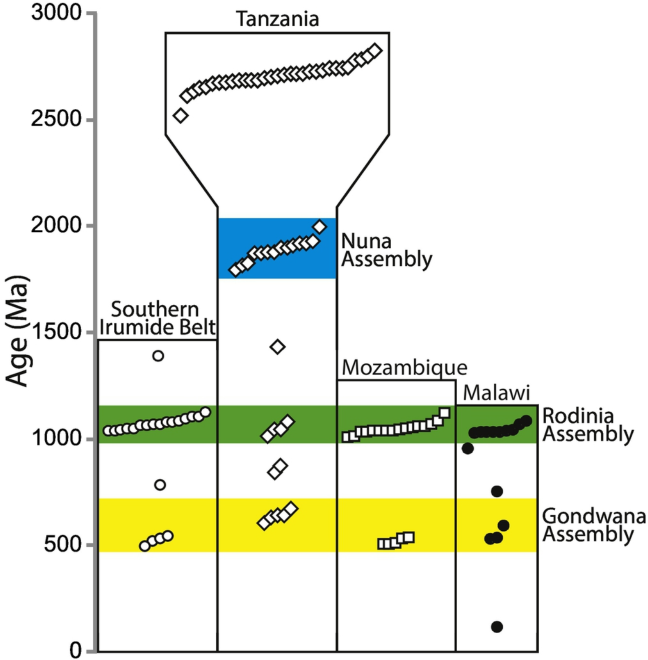

3000
2500
2000
1500
1000
500
0
Age (Ma)
Tanzania
Nuna
Assembly
Southern
Irumide Belt
Mozambique
Malawi
Rodinia
Assembly
Gondwana
Assembly

Figure 6